TOXICOLOGIC PATHOLOGY, vol 30, no 3, pp 373–389, 2002
Copyright © 2002 by the Society of Toxicologic Pathology

Air Pollution and Brain Damage

LILIAN CALDERÓN-GARCIDUEÑAS,[1,2] BIAGIO AZZARELLI,[3] HILDA ACUNA,[2] RAQUEL GARCIA,[2] TODD M. GAMBLING,[4] NORMA OSNAYA,[2] SYLVIA MONROY,[2] MARIA DEL ROSARIO TIZAPANTZI,[2] JOHNNY L. CARSON,[4] ANNA VILLARREAL-CALDERON,[2] AND BARRY REWCASTLE[5]

[1]*Curriculum in Toxicology, University of North Carolina at Chapel Hill, North Carolina 27599-7310, USA*
[2]*Instituto Nacional de Pediatria, Mexico City, 14410, Mexico*
[3]*Pathology Department, Indiana University, Indianapolis, Indiana 46202-5120, USA*
[4]*Center for Environmental Medicine and Lung Biology, University of North Carolina at Chapel Hill, North Carolina 27599-7310, USA, and*
[5]*Pathology Department, Foothills Hospital, Calgary, Alberta, T2S0R3, Canada*

ABSTRACT

Exposure to complex mixtures of air pollutants produces inflammation in the upper and lower respiratory tract. Because the nasal cavity is a common portal of entry, respiratory and olfactory epithelia are vulnerable targets for toxicological damage. This study has evaluated, by light and electron microscopy and immunohistochemical expression of nuclear factor-kappa beta (NF-κB) and inducible nitric oxide synthase (iNOS), the olfactory and respiratory nasal mucosae, olfactory bulb, and cortical and subcortical structures from 32 healthy mongrel canine residents in Southwest Metropolitan Mexico City (SWMMC), a highly polluted urban region. Findings were compared to those in 8 dogs from Tlaxcala, a less polluted, control city. In SWMMC dogs, expression of nuclear neuronal NF-κB and iNOS in cortical endothelial cells occurred at ages 2 and 4 weeks; subsequent damage included alterations of the blood–brain barrier (BBB), degenerating cortical neurons, apoptotic glial white matter cells, deposition of apolipoprotein E (apoE)-positive lipid droplets in smooth muscle cells and pericytes, nonneuritic plaques, and neurofibrillary tangles. Persistent pulmonary inflammation and deteriorating olfactory and respiratory barriers may play a role in the neuropathology observed in the brains of these highly exposed canines. Neurodegenerative disorders such as Alzheimer's may begin early in life with air pollutants playing a crucial role.

Keywords. Air pollution; Mexico City; canines; Alzheimer's; nasal epithelia; BBB; NFκB; iNOS.

INTRODUCTION

A complex mixture of gases, particulate matter (PM), and chemicals present in outdoor and indoor air produces adverse health effects. Because the nasal cavity is a common portal of entry for such pollutants, the nasal olfactory and respiratory mucosae are vulnerable to damage and well-known targets for air pollutant-induced toxicity and carcinogenicity (55, 85, 86, 91). The nose-brain barrier depends on intact epithelia, including tight junctions and an intact xenobiotic metabolizing capacity (37). Olfactory receptor cell dendrites are in direct contact with the environment, and, thus, pinocytosis and neuronal transport are likely routes of access to the central nervous system (CNS) of potential toxins (75). Olfactory receptor neurons project from the sensory epithelium to targets within the olfactory bulb, the first synaptic relay in the olfactory pathway (75). The mucociliary apparatus of the respiratory mucosa also functions as a barrier to protect against neuronal uptake and transport by trapping insoluble inhaled material in a layer of secretions that are in continuous movement towards the nasopharynx (85). The contribution of air-pollutant exposure to airway epithelial injury is well documented.

Healthy children and adult populations in Southwest Metropolitan Mexico City (SWMMC)—an urban area characterized by significant daily concentrations of pollutants such as ozone, PM, and aldehydes—have shown extensive damage to the respiratory nasal epithelium (24–26, 27). Children in SWMMC display ultrastructural evidence of deficiencies in nasal epithelial junction integrity, cytoplasmic deposition of PM, and altered mucociliary defense mechanisms (27). Canines living in SWMMC exhibit similar nasal respiratory lesions (unpublished observations, Calderón-Garcidueñas), along with respiratory bronchiolar and myocardial pathology (20, 22). A sustained pulmonary inflammatory process is clearly seen in exposed canines (22), and SWMMC children show radiological and spirometric evidence of lung damage and cytokine imbalance (23). Impaired olfaction, hyposmia, or anosmia are important early changes in neurodegenerative diseases including Alzheimer's (AD) and Parkinson's disease (PD) (58, 66, 114), as well as in aging (57, 59). All layers of the olfactory bulb are affected in

Address correspondence to: Lilian Calderón-Garcidueñas, Department of Environmental Sciences and Engineering, The University of North Carolina at Chapel Hill, 348 Rosenau Hall CB #7431, Chapel Hill, North Carolina 27599-7431; e-mail: liliancalderon888@hotmail.com .

0192-6233/02$3.00+$0.00

aging and AD, and olfaction is impaired in the early stages of AD (66, 67).

Aged canines are valuable models of aging (16, 36). Veterinarians have noticed geriatric behavioral changes in pet dogs including decrements in attention and activity, wandering and disorientation, and disturbances of the sleep/wake cycle (36, 98). In aged dogs, beta-amyloid accumulation correlates with cognitive dysfunction; plaques are of the diffuse subtype; and there is no neuritic involvement (36). A threshold effect of plaque development was observed by Russell (99) in 103 laboratory-raised beagles. In dogs kept in outdoor kennels at Davis, CA, and Fort Collins, CO, no plaques were apparent at ages younger than 10 years, but numbers progressively increased to 73% at ages 15 to 17.8 years (99). Weigel (111) described in a cohort of 30 mongrel dogs a subpopulation with increased numbers of β-amyloid-positive diffuse plaques and concluded that only 43% of these mongrel dogs were susceptible to amyloidosis or that only the severely affected subpopulation was exposed to a factor or factors inducing this pathology. Fibers representing an early neuritic change that precedes tau hyperphosphorylation have been described by Satou et al (101) in aging dogs.

This report describes early and progressive alterations in the nasal respiratory and olfactory mucosae, the olfactory bulb, and cortical and subcortical brain structures in healthy dogs in SWMMC exposed daily to high levels of ambient air pollutants; canines from a comparable city, Tlaxcala, with low levels of pollution represent controls. Early changes included nuclear factor-kappa beta (NF-κB)- and inducible nitric oxide synthase (iNOS)-positive cells, vascular changes in cortical small arterioles and capillaries, apoptosis in glial and vascular smooth muscle cells and pericytes, cortical perineuronal satellitosis, and neuronal chromatolysis. These alterations were followed by reactive astrocytosis predominantly in cortical white matter and subpial regions, apolipoprotein E (apoE) immunoreactivity in abnormal lipid vacuoles in blood vessels, and astrocytic processes, nonneuritic plaques, and neurofibrillary tangles (NFT).

MATERIALS AND METHODS

Study Areas

Clinically healthy mongrel dogs from Tlaxcala and SWMMC were studied. The selection of the 2 different cities was based on their concentrations of air pollutants and similar altitudes above sea level. Metropolitan Mexico City extends over 2,000 km^2 and is located in an elevated valley, 2,250 m above sea level. It is a megacity with 20 million residents and the associated production of air pollutants from automobiles, leakage of petroleum gas, and industrial activity. The climate is mild with year-round sunshine, light winds, and temperature inversions. Each of these factors contributes to create an environment in which complex photochemical reactions produce oxidant chemicals and other toxic compounds. Air quality data are provided by an automated surface network of 33 monitoring stations in and around MC; hourly, near-surface measurements are made of monitored pollutants including ozone, PM_{10}, SO_2, NO_2, CO, and Pb. Mexico City's main pollutants are PM and ozone, with levels exceeding US National Ambient Air Quality Standards (NAAQS) most of the year. The maximal concentrations of ozone precursors appear downwind of the emission zones toward the southern urban area, southwest and southeast MC (47). According to Fast and Zhong (43), the highest particle concentrations occur regularly in the vicinity of the peak ozone concentrations during the afternoon. Ozone concentrations as high as 0.48 ppm have been measured during severe air pollution (13); the SWMMC atmosphere is characterized by average maximal ozone daily concentrations of 0.250 ppm. An average of 4 ± 1 hr/day with ozone >0.08 ppm is recorded in SWMMC year-round (83.9% of days) (47). NO_2 concentrations do not usually exceed the annual arithmetic mean of 0.053 ppm (4.6% of days), whereas SO_2 levels exceed the 24-hr primary standard of 0.14 ppm in the winter months. Both PM_{10} and $PM_{2.5}$ exceed their respective annual arithmetic means above the standards (annual NAAQS PM_{10} 78 $\mu g/m^3$ and $PM_{2.5}$ 21.6 $\mu g/m^3$ vs standards of 50 $\mu g/m^3$ and 15 $\mu g/m^3$, respectively) (31, 41). Other pollutants detected in SWMMC include volatile organic compounds (VOC), such as linear and cyclic saturated and unsaturated hydrocarbons (HC); aromatic HC; aldehydes; ketones; esters; and acids and their halogenated derivatives (77). Formaldehyde and acetaldehyde ambient values are in the range of 5.9 to 110 ppbv, and 2 to 66.7 ppbv, respectively (5). Mutagenic particulate matter (108); alkane hydrocarbons (13); benzene (81); various metals such as vanadium, manganese, and chromium (96); and peroxyacetyl nitrate (41) are also detected. Lichens absorb their nutrients from the atmosphere and can be used as sensitive monitors of airborne metals (107); *Parmotrema arnoldii* accumulates lead, copper, and zinc in SWMMC (77). In addition, 500 metric tons of canine fecal material are deposited daily on MC streets (28).

The rationale behind selecting the SW geographical area in MC involved 2 major factors. First, the spacial distribution of pollutants such PM_{10}, O_3, SO_2, and NO_2 within the city reflects the higher concentrations of particulate and gaseous emissions in the northern part of the city where most industries are located. Ozone levels are higher in the south, a residential area, as a result of wind transport of the mass precursor pollutants emitted in the industrial northern and central regions. Second, our studies of healthy children and adults living in SWMMC present evidence of nasal and pulmonary pathology, as well as serum cytokine imbalance in children (21, 23).

Tlaxcala was selected as the control city because its altitude above sea level is similar to that of MC, and studies in canines from this area have shown minimal pulmonary and cardiac pathology (20, 22). Tlaxcala is the capital city of the state of Tlaxcala, located 114 km east of Mexico City at 2,252 m above sea level. It has a temperate climate, an average temperature year-round of 16°C, and 700 mm of annual rainfall. With 63,423 inhabitants, it is a city in compliance with current air pollution regulations.

Atmospheric Pollutant Data

Mexico City's atmospheric pollutant data were obtained from the available literature and a representative monitoring station located in the SW. Tlaxcala's data were obtained from the Subsecretaria de Ecologia. SWMMC data represent air pollution patterns corresponding to the ages of the dogs and tissue collection times (2000–2001).

TABLE 1.—Physical descriptions of Tlaxcala control and SWMMC canines.

Age	Control (gender)	SWMMC (gender)	Average weight
24–48 h	0	4 (2F/2M)*	275 ± 120 g
2–4 wk	0	3 (1F/2M)*	554 ± 190 g
1 and 3 mo	0	2 (M)*	460 g and 7 kg
8–12 mo	2 (1F/1M)	2 (M)*(F)	11.2 ± 2.4 kg
>1 yr to <3 yr	2 (1F/1M)	4 (2F/2M)	12.16 ± 5.74 kg
4–5 yr	1 (F)	4 (2F/2M)	20.3 ± 5.2 kg
6–8 yr	2 (F)	11 (7F/4M)**	22.0 ± 8.6 kg
11 and 12 yr	1 (F)	2 (1F/1M)	37.33 ± 11.01 kg
Total	8	32	

*Animals raised at the animal facility outdoor/indoor kennel.
**Two males ages 6 and 7 also raised at the animal facility.

Canine Population

Physical descriptions of the mongrel dogs used for this study (18M/22F)—8 from Tlaxcala and 32 from SWMMC—are presented in Table 1. The younger SWMMC dogs ($\leq$1 year) and 2 of the older dogs were whelped and continuously housed in an outdoor-indoor kennel. The remaining older (>1 yr) SWMMC dogs and all the Tlaxcala dogs were home-raised and kept continuously outdoors. These dogs were periodically seen by a veterinarian, received all of the applicable vaccinations, and were dewormed regularly. They were fed twice daily with a combination of owners' choice commercial dog chow and home food leftovers and had free access to potable water. These dogs had no contact with other animals, lived permanently in the selected residential area, and received no exposures to local toxins such as paints, metals, and solvents. Dogs kept in an outdoor-indoor kennel were housed 1 dog per run, fed once a day (Purina Dog Chow, Ralston-Purina, Cuautitlan, Mexico), and provided water ad libitum. They were under close clinical veterinary observation during their entire lives, and at no time was there any evidence of overt respiratory, cardiovascular, or neurological disease. None of the dogs had been outside their residential area or lived in a different city.

The study protocol was reviewed and approved by the Basic Research Committee of the Instituto Nacional de Pediatria in Mexico City. Husbandry was in compliance with all regulations of the American Association of Laboratory Animal Certification (AALAC). We applied the dementia index suggested by Uchino (105) to all participant dogs, except those younger than 3 months. Euthanasia was conducted in accordance with established guidelines and applicable animal care-and-use regulations (92).

Necropsy and Tissue Preparation

Animals were examined by a veterinarian before they were euthanized. A brief clinical exam included cardiac and pulmonary auscultation, an abdominal and peripheral lymph node palpation, and a neurological examination. Whole blood was taken for a complete complete blood count (CBC). Each dog was sedated with IV xilazine (Rompum, Bayer, Leverkusen, Germany) and then deeply anesthetized with sodium pentobarbital (Salud y Bienestar, Mexico). A gross external description was noted after their demise; animals were weighed; and a complete necropsy was performed. Immediately after death, the skull was opened and the olfactory bulbs and brain removed. Nasal tissues including the nasoturbinate, maxilloturbinate, and ethmoturbinate mucosae (including the olfactory epithelium) were carefully dissected; the anatomical regions were identified; and tissues from specific anatomical areas were labeled separately. Separate sets of these tissues and the olfactory bulbs were immediately immersed in 2 types of fixatives for EM and LM, respectively: 4% paraformaldehyde and 0.1% glutaraldehyde in 0.1M phosphate buffer at pH 7.4, and 10% neutral formaldehyde. The base of the skull was inspected for gross abnormalities. The brain was carefully examined, and alternating right and left cerebral hemispheres were quickly frozen and stored at -80°C for future studies. The uncut hemisphere and the remaining portions of the brain stem and cerebellum were fixed in 10% neutral formaldehyde for 2 weeks. Paraffin sections for light microscopy (LM) were then cut from the following regions: frontal (sigmoides anterior and posterior), postcruciate gyrus, gyrus coronalis, gyrus ectolateralis, posterior suprasylvian gyrus gray and white matter, hippocampus, entorrhinal cortex, olfactory bulbs, cerebellum, caudate nuclei, thalamus, hypothalamus, midbrain, pons, and medulla. The location of the sample in each of these regions was standardized in every brain. The trachea, extrapulmonary bronchi and lungs, and heart were excised intact from the thoracic cavity, and the abdominal cavity was opened and examined. In a group of 14 dogs (7 from each city) matched by age and gender, frontal lobe samples were processed for electron microscopy (EM). Samples of liver, spleen, and kidneys were obtained and immediately immersed in 10% neutral formaldehyde. Other sections were cut from the caudal and cranial lung lobes, peribronchial and peritracheal lymph nodes, right and left ventricles, interventricular septum, atrium, and pancreas.

Paraffin sections 5-um thick were cut and stained routinely with hematoxylin and eosin. Special stains included a modified Bielschowsky silver stain, Congo red, thioflavin-S, periodic acid methenamine silver (PAM), and periodic-acid-Schiff (PAS). Apoptosis was evaluated through analysis of nuclear and cellular morphology (LM and EM) and DNA fragmentation. The terminal deoxynucleotidyl transferase (TdT) labeling assay (TUNEL, ApopTag, Intergen Company, New York, NY) was used to assess cells with DNA strand breaks (72). Immunohistochemistry (IHC) was performed using the following antibodies at the indicated dilutions: GFAP, 1:100 (Boehringer Mannheim, Indianapolis, IN, USA); apolipoprotein E (apoE), 1:500 (Biodesign, Saco, Maine, USA); tau AT8 phosphorylated Ser-202 and Thr-205, 1:300 (Innogenetics, Alpharetta, GA, USA); NF-κB p65 transcription factor, 1:100 (Transduction Laboratories, Lexington, KY, USA); anti-macNOS (macrophage inducible iNOS) mAB N32030, 1:500 (Transduction Laboratories, Lexington, KY); and CD68 KP1, 1:100 (Novocastra Laboratories, Newcastle upon Tyne, UK). Briefly, 5 μm paraffin sections were dried overnight, deparaffinized in xylene, and rehydrated through graded alcohols. Slides were immersed in 10 mM citrate buffer (pH 6.0) and heated in a microwave oven, 4 cycles of 5 minutes each, to unmask antigenic sites. Thereafter, slides were removed and cooled for 15 minutes at room temperature before washing in PBS. Endogenous peroxidase activity was inhibited by rinsing slides in 0.1% hydrogen peroxide for 10 minutes. Following washing in PBS, sections were incubated overnight at 4°C with antiserum. Immunohistochemical localization was performed

using an avidin-biotinylated peroxidase complex method (Vectastain ABC kit, Vector Laboratories, Burlingame, CA). Negative controls included utilization of nonspecific IgG instead of the primary antibodies and preabsorbtion of primary antibodies with the respective cognate peptides. The histopathologic severity of the brain findings was assessed semiquantitatively using grades from 0–3 [0) no pathological change, 2) moderate change to 3) most severe]. The parameters evaluated included the presence of histological elements characteristic of neuronal, glial necrosis or apoptosis; the distribution and characteristics of astrocytes (H&E, GFAP, and NF-κB p65), microglia (H&E), and oligodendroglia; and vascular changes (H&E and 1-um toluidine-blue sections). The olfactory epithelium was evaluated using the terminology suggested by Hardisty et al (54) for rat olfactory tissues. Pathological findings were divided into 5 categories: degeneration, regeneration, postdegenerative atrophy, inflammation, and respiratory metaplasia/basal cell hyperplasia. The grading system scored pathology as follows: 0) within normal limits, 1) minimal (apparent loss of a few sensory cells), 2) mild (focal loss of sensory cells with some sustentacular or other cellular damage involving up to about 25% of the olfactory mucosa in the section), 3) moderate (more extensive epithelial damage or lesions extending into the lamina propia to involve Bowman's glands or other structures, with up to 50% of the olfactory mucosa in the section involved); 4) marked (up to 75% of the olfactory mucosa in the section involved; other tissue changes occur, such as inflammation or edema, in addition to sensory cell loss, sustentacular cellular and/or Bowman's gland acinar ablation); and 5) severe (complete loss of olfactory mucosa in the affected area along with changes that might inhibit repair, such as loss of basal cells in association with epithelial erosion or ulceration). Sections were read blindly by experienced observers with no access to the codes regarding the geographical source of the animals. Light and electron microscopic images were transmitted to Adobe Photoshop 4.0 using a Nikon scanner.

Statistics was performed using the Instat program (Graph Pad, San Diego, CA). Differences in the hematological parameters between control and exposed dogs were tested with the unpaired *t*-test. Significance was assumed at $p < 0.05$. Data are expressed as mean values $\pm$ SD.

RESULTS

Air Quality Data

People and animals in Mexico City are chronically exposed to a complex mixture of air pollutants. The numbers of hours per year that SWMMC residents have been exposed to ozone above the USNAAQS for the years 1984–1998 are: 40, 30, 740, 959, 1,224, 1,403, 1,561, 1,395, 1,146, 1,061, 1,249, 1,080, 1,123, 1,203, and 1,342, respectively. The marked increase in the number of daily ozone excesses in Mexico City initially started in the fall of 1986 when the atmospheric air deteriorated from highly reductive to oxidative, coinciding with the introduction of a new gasoline with a tetraethyl lead concentration of 0.64 ml/gal (47). In 1989, a new change in reactivity of the emitted VOCs occurred following the introduction of methyl-*t*-butyl ether (MTBE) to Mexico City gasolines (18). Figure 1 illustrates the average daily concentrations of ozone (ppm), PM_{10} (ug/m^3), NO (ppb), NO_2 (ppb), SO_2 (ppb), CO (ppm), relative humidity (%) and temperature (°C) for the year 2000. PM_{10} and $PM_{2.5}$ exceeded their respective NAAQS (annual PM_{10} 78 ug/m^3 and $PM_{2.5}$ 21.6 ug/m^3 vs standards of 50 ug/m^3 and 15 ug/m^3), respectively (31, 41).

Clinical and Gross Pathological Observations

The two older dogs from our SWMMC animal facility, males ages 6 and 7 years, exhibited decrements of attention and activity and disturbances of the sleep/wake cycle during the year preceding the study; one of them already had predementia scores (Table 2). The caretakers reported transient episodes during which the dogs failed to recognize their habitual caretakers and would sporadically show short episodes of decreased body language. No changes in food intake were noted, and their weights remained stable. Using the Uchino et al criteria for evaluation in dogs (105), all Tlaxcala control animals showed scores of 10 corresponding to normal. SWMMC animals, except the 7-year-old with a score of 29, had scores still within the normal range (10–21); however, caretakers were aware of alterations of sleep patterns and barking.

All of the animals in this study were healthy without evidence of overt neurological, respiratory, or cardiovascular disease. There were no overweight dogs. For 2 of the SWMMC dogs, ages 3 and 8 yr, owners reported occasional epistaxis that did not require veterinary attention. The results of the CBCs are shown in Table 3. There was a significant difference ($p < 0.0001$) in the numbers of monocytes between controls (3.02 ± 1.4) and exposed (10.36 ± 3.28).

Lungs from MC dogs displayed patchy whitish pleural areas with scattered anthracotic macules. These pleural changes were seen in every lobe and had no apparent relationship with the ribs or lung apices. The changes were particularly prominent in older dogs (>5 years). Enlarged, congested, anthracotic pulmonary hiliar lymph nodes were observed in all MC dogs. No evidence of intercurrent lung disease was seen in any of the animals. The hearts showed no gross abnormalities. No other gross abnormal findings were seen, with the exception of small calculi in the pyelocalyceal system of the SWMMC 12-year-old dog.

Non-Central Nervous System (CNS) Findings

Pulmonary Histopathology: Dogs from Tlaxcala exhibited scattered minute anthracotic pleural areas and discrete areas of pleural thickening. SWMMC dogs showed respiratory bronchiolar epithelial hyperplasia; smooth muscle hyperplasia was salient in terminal and respiratory bronchioles (Figure 2A). Chronic mononuclear cellular infiltrates along with macrophages loaded with PM commonly surrounded the bronchiolar walls and extended into adjacent vascular structures (Figure 2A). NF-κB was seen in the nuclei of alveolar type II cells and cytoplasm of alveolar macrophages in all SWMMC animals starting at age 4 weeks. In lung-associated lymph nodes, a distortion of the normal architecture with dilatation of peritrabecular and subcapsular sinuses occurred, and a mixture of coal-like particles and brown–yellow, birefringent particles was present in macrophages. Tlaxcala dogs exhibited mild bronchiolar epithelial hyperplasia along with focal smooth muscle cellular hyperplasia. Alveolar macrophages with PM were present in small

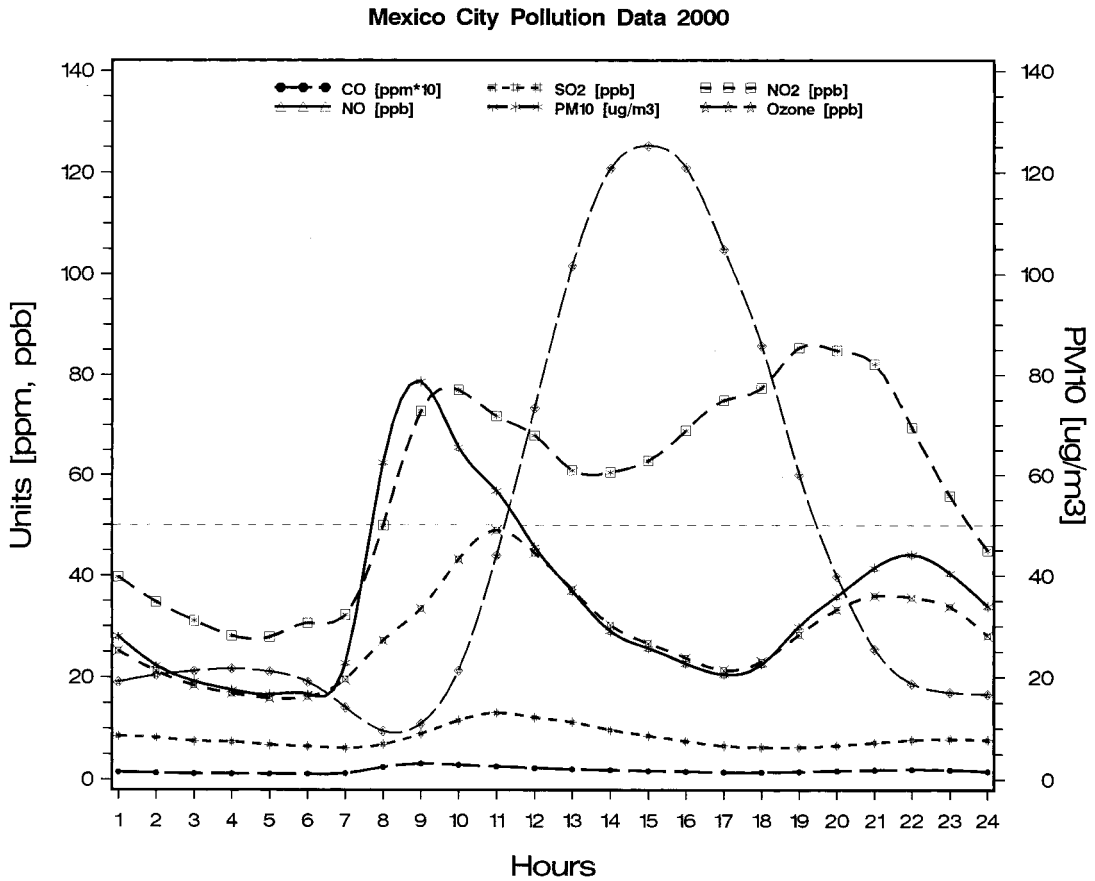

FIGURE 1.—SWMMC air pollutant data, daily averages, year 2000; main pollutants included. Notice that animals and people exposed to the SWMMC environment are sequentially exposed to significant concentrations of ozone, PM_{10}, and nitrogen oxides (NO). The dashed horizontal line marks the PM_{10} annual standard (50 ug/m^3). The two main pollutants above the current standards are ozone and PM_{10}.

numbers, and rare foci of inflammatory cells were seen in association with either terminal bronchioles or pulmonary blood vessels.

Nasal Histopathology Respiratory Epithelium: Young Tlaxcala dogs showed unremarkable pseudostratified ciliated columnar epithelium with goblet cells, whereas older dogs had focal areas of squamous metaplasia and mild-to-moderate thickening of the basement membrane. SWMMC dogs younger than 3 months displayed unremarkable respiratory nasal epithelium. Changes in SWMMC dogs became progressively worse with age and were characterized by extensive replacement of the mucociliary epithelium by focal globet cell hyperplasia in younger dogs, followed by replacement of the ciliated goblet cell epithelium by squamous metaplastic epithelium with scattered intraepithelial polymorphonuclear leucocytes (PMNs) (Figure 2B, C). iNOS granular positivity in ciliated epithelial cells was observed in all dogs (controls and SWMMC) with intact respiratory epithelium. In dogs with squamous metaplastic changes, however, the iNOS positivity extended to include the full thickness of the epithelium (Figure 2C). The submucosal glands exhibited dilatation and atrophy in a few cases, and there were numerous glands with strong iNOS positivity in SWMMC dogs (Figure 2C). In addition, marked thickening of the basement membrane and a predominantly chronic, discrete, inflammatory submucosal infiltrate were observed.

TABLE 2.—Total scores for the Dementia Index for control and SWMMC dogs.*

Age	Controls (average score)	SWMMC
<3 yr	10	10
4–5 yr	10	15
>6–8 yr	10	16
11 and 12 yr	10	28

*Criteria of Uchino (105) for evaluation of dementia in dogs: 10–21 normal, 21–29 predementia, >29 dementia.

Nasal Histopathology Olfactory Epithelium: Sections from the endoturbinate regions III and IV representative of olfactory epithelium (82) were identified and compared in the different dogs. Grossly, the olfactory region showed a distinct yellowish-brown color in Tlaxcala and the younger SWMMC dogs. Older dogs in Tlaxcala and SWMMC exhibited a grayish discoloration of the olfactory area. Microscopically, the neurosensory epithelium was intact and well defined in all control dogs and SWMMC dogs younger than 3 months. Microscopic changes were detected in SWMMC young dogs, the earliest in the 8-month-old. The changes were focal and characterized by disruption of the orientation of the sensory olfactory and sustentacular cells as well as degeneration with loss of both of these cell types, resulting in a decrease in the

TABLE 3.—CBC hematological data for control and SWMMC canines >1 year.

Groups	Hb	Ht	WBC	Lymph	Monos*	PMN	PlateIt	MPV
Control	15.4 ± 2.7	44.8 ± 7.6	14.5 ± 3.1	45.9 ± 38.5	3.0 ± 1.4	29.6 ± 30.5	291,000 ± 17900	9.2 ± 1.1
SWMC	15.7 ± 2.4	48.4 ± 7.4	12.4 ± 4.7	78.5 ± 10.9	10.3 ± 3.2	7.1 ± 5.0	248,000 ± 72000	10.4 ± 1.4

*$p < 0.0001$.

thickness of the neuroepithelium (Figure 2D). Production of pseudoglandular cyst-like structures was seen sporadically; however, proliferation of undifferentiated cells originating from the basal layer was rare. The changes became progressively worse in older animals (>5 years) where large patches of olfactory mucosa were thin and devoid of any architectural orientation. Pyknotic nuclei and scattered PMNs and mononuclear cells were observed at all levels of the altered

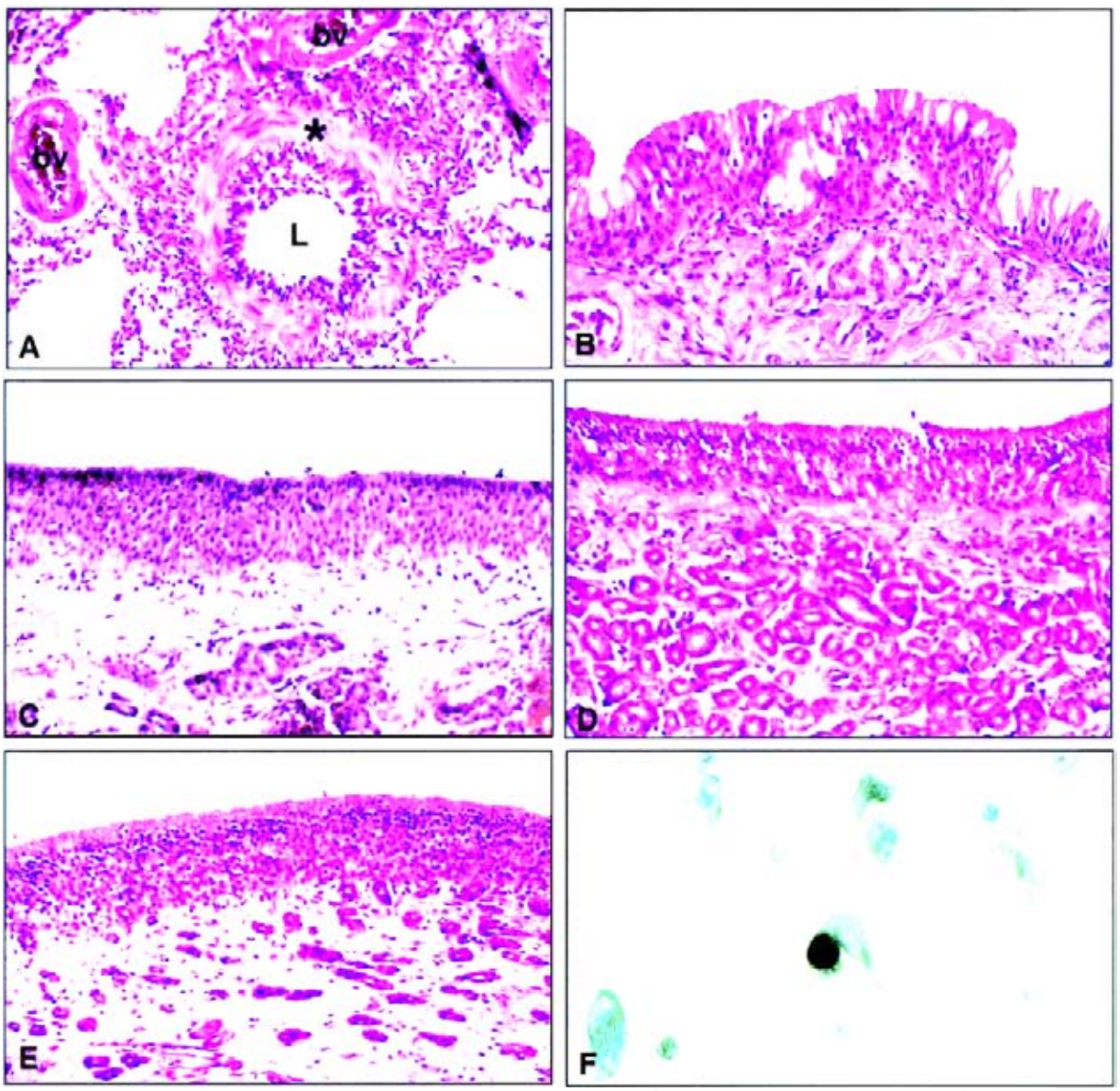

FIGURE 2.—SWMMC dogs. 2A) Respiratory bronchiole, 3-year-old. Note the striking smooth muscle cell hyperplasia (black*) and desquamated bronchiolar cells in the lumen. A chronic mononuclear cell infiltrate with numerous macrophages loaded with particulate matter (white*) is seen in the peribronchiolar region and extends to adjacent blood vessels (bv). H&E. ×107. 2B) Nasal respiratory epithelium, 1-year-old. The epithelium is variably thickened and contains abundant goblet cells and a paucity of ciliated cells. Inflammatory cells have infiltrated the epithelium and submucosa. H&E. ×214. 2C) Nasal respiratory epithelium, 3-year-old. The normal mucociliary epithelium has been replaced by a metaplastic squamous epithelium with strong iNOS expression. ×214. 2D) Olfactory epithelium, same dog as 2B. There is focal loss of sensory and sustentacular cells without evidence of regeneration. The basement membrane is thickened, and a few chronic inflammatory cells are present in the submucosa. H&E. ×214. 2E) Olfactory epithelium, same dog as 2C. There are epithelial disorganization and paucity of Bowman's glands. H&E. ×214. 2F) Olfactory bulb. A glial cell apoptotic nucleus is seen in close contact with a neuron. TUNEL. Lightly counterstained with methyl green. ×420.

TABLE 4.—Olfactory epithelial histopathology in control and SWMMC canines.

Histopathopathology	Groups	0	1	2	3	4
Olfactory epithelium*	Control					
	SWMMC					
Degeneration	Control	5	3	0	0	0
	SWMMC	9	17	4	2	0
Regeneration	Control	7	1	0	0	0
	SWMMC	14	12	5	1	0
Postdegenerative atrophy	Control	7	1	0	0	0
	SWMMC	29	2	1	0	0
Inflammation	Control	6	2	0	0	0
	SWMMC	10	20	2	0	0
Respiratory metaplasia	Control	5	3	0	0	0
	SWMMC	15	12	1	3	1
Basal cell hyperplasia	Control	8	0	0	0	0
	SWMMC	32	0	0	0	0

*Descriptive terminology based on Hardisty et al (54) for rat olfactory tissues.

epithelium and in the submucosa (Figure 2D). The basement membrane was thickened, and an increase in loose connective tissue was noticed in older animals (Figure 2D). In some areas there was focal replacement of the degenerative neurosensorial epithelium by squamous metaplastic epithelium. Tubuloacinar olfactory glands were intact in younger SWMMC and control animals; however, SWMMC dogs older than 1 year showed scattered hyperchromatic nuclei and deposition of abundant gold-brown pigment in the cytoplasm. Areas with atrophic Bowman's glands surrounded by loose connective tissue were focally prominent (Figure 2E). Bundles of unmyelinated olfactory nerve fibers and myelinated nerve fibers (trigeminal nerve) were unremarkable in Tlaxcala dogs $\leq$3 years and the younger SWMMC canines; however, in SWMMC dogs older than 5 years, the degeneration of the sensory and sustentacular cells was accompanied by an apparent loss of nerve bundles in the lamina propria. Strongly positive iNOS staining was seen in the slender apical portion of the neurosensory neurons projecting to the surface of the epithelium, as well as in the ducts of the olfactory glands coursing through the propia and epithelium. A summary of the olfactory epithelial findings is presented in Table 4.

CNS Findings

All dogswere mesaticephalic except one—a mixed collie breed that was dolichocephalic. Brains were cut on the coronal plane, and there was no evidence of ventricular dilatation or cortical atrophy in any animal. The leptomeninges were thickened in SWMMC animals older than 8 years; however, the change was minimal. A summary of neuropathological findings is seen in Table 5.

Brain Histopathology Olfactory Bulbs: Apoptotic cells, seen in the different layers in all control and exposed animals, were rare in controls and few to moderate in exposed dogs. They corresponded mainly to glial cells (Figure 2F). Reactive astrocytosis present in all layers (including external and internal plexiform layers, mitral cell layer, and the olfactory glomeruli) varied in intensity but was seen in every SWMMC dog starting at age 8 months. Senile plaques and NFTs were not seen by tau and modified Bielschowsky silver stain. Vascular changes characterized by foamy yellowish structures in the walls of small arterioles and capillaries were better defined in 1-um-thick, toluidine blue, plastic-embedded sections, and displayed the same features as the vascular changes described in cortical areas. Except for a few white matter reactive astrocytes in the older control dogs, the olfactory bulbs were unremarkable.

Brain Histopathology Cortical Sections: Astrocytes with a small amount of eosinophilic cytoplasm were seen around blood vessels and neurons in young SWMMC dogs. These astrocytes were predominantly cortical and did not stain with GFAP. Reactive astrocytes were focally prominent in subpial areas of all SWMMC animals starting at age 8 to 12 months; positive GFAP processes could be seen along penetrating cortical blood vessels. Very few GFAP-positive astrocytes were seen in the gray matter regardless of the age of the dog; however, the white matter showed progressively increased numbers of reactive astrocytes. In the younger animals the positive processes were restricted to perivascular areas (Figure 3A); in the older animals (>5 years) the reactive astrocytes were abundant in the neuropil without any obvious relationship with blood vessels (Figure 3B). A few multinucleated astrocytes were scattered in the white matter of older dogs, and some showed hyperchromatic nuclei. Foci of satellitosis and chromatolysis were observed in the cortical gray and appeared more prominent in frontal and entorrhinal cortices. Neurons in layers III-VI showed dark, shrunken cytoplasmic bodies surrounded by numerous glial nuclei; up to 8 nuclei were seen (Figure 3C). Large pyramidal neurons were particularly affected. Neuronal changes with satellitosis were seen in the 8- and 12-month-old dogs.

The paucity of frontal neurons was remarkable in $\geq$4-year-old dogs (Figure 3D). TUNEL revealed positive astrocytic and oligodendroglial nuclei in close relationship with dark neurons. In younger dogs apoptotic cells were restricted to perivascular areas, predominantly in the white matter. No neurons showed positive TUNEL nuclei. Older animals (>5 years) exhibited numerous apoptotic nuclei both in the white matter and, to a lesser degree, in the cortex. Control animals exhibited a rare apoptotic nucleus in the white matter. Microglial cells with ameboid profiles could be seen in the cortex and white matter. Scattered cortical ameboid microglia could be seen as early as 8 months; however, their number increased with age, particularly in the gray matter. Endothelial cells exhibited a granular cytoplasmic staining with the CD68 antibody, and a few pyramidal neurons also exhibited

TABLE 5.—Summary of neuropathological findings in SWMMC canines.

Age groups	NF-κB nuclear	NF-κB glial	iNOS	Neuronal changes	LM vascular pathology	Apoptosis	GAFP	NFT*	Nonneuritic plaques
0–3 mo (n = 9)	+	0	0	0	0	0	0	0	0
8 mo to 3 yr (n = 6)	+	+	+	+	+	+	+ perivascular	0	0
4–8 yr (n = 15)	+	++	++	++	++	++	++	+	+
11–12 yr (n = 2)	+	++	+++	+++	+++	++	++	+	+

*Tau and modified Bielschowsky silver stain.

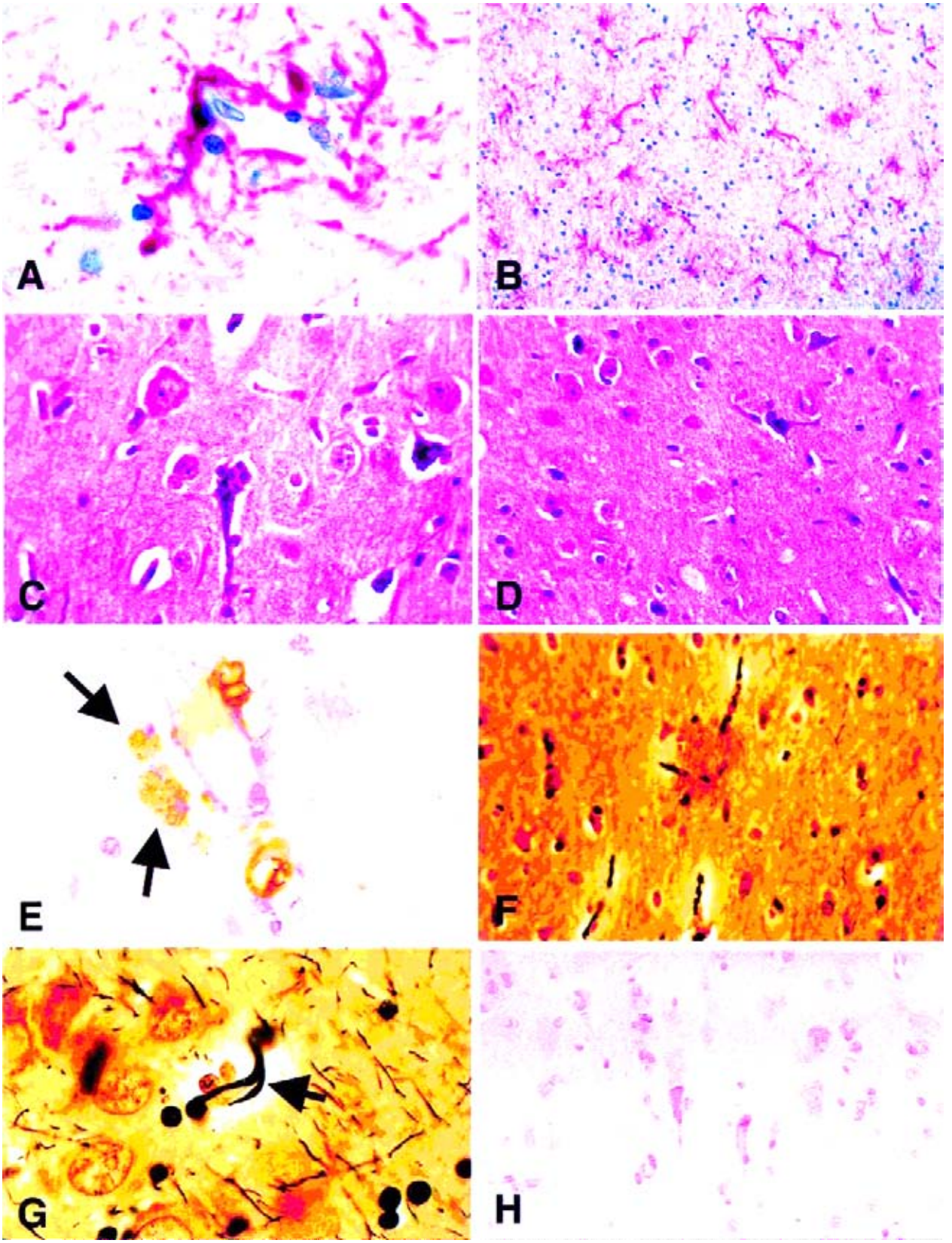

FIGURE 3.—SWMMC dogs. 3A) Frontal white matter, 3-year-old. GFAP-positive astrocytic processes are seen primarily around blood vessels. Light counterstaining with hematoxylin. ×420. 3B) Frontal white matter, 12-year-old male with predementia scores. There is a moderately reactive astrocytosis. GFAP. ×42. 3C) Frontal cortex, 4-year-old. Dying neurons exhibit condensation of both cytoplasm and nuclei, are surrounded by numerous glial cells, and do not develop apoptotic bodies. H&E. ×420. 3D) Frontal cortex, 4-year-old. Nerve cell loss and numerous microglia-like ameboid cells are apparent. H&E. ×214. 3E) Frontal cortex, 6-year-old. Strong positive apoE staining is present in lipid deposits located in blood vessel walls; two macrophages (arrows) exhibit abundant granular positive staining. ×1072. 3F) Frontal cortex, 7-year-old. An argyrophilic non-neuritic plaque is present in the center of the photomicrograph. Modified Bielschowsky silver stain. ×214. 3G) Parahippocampal gyrus, 8-year-old. A tangle (arrow) appears as dark bands curving through the cytoplasm of the neuron. Modified Bielschowsky silver stain. ×420. 3H) Frontal cortex, 4-year-old. Pyramidal neurons show weak tau AT8—positivity. No counterstain. ×107.

a weak granular positive cytoplasmic staining. ApoE was particularly prominent in relation to the lipid vacuoles in cortical and subcortical blood vessels and could be seen in neurons, astrocytes, and perivascular macrophages (Figure 3E). Rare nonneuritic plaques and NFTs were seen with the modified Bielschowsky silver stain in 3 SWMMC dogs ages 7, 8, and 12 (Figures 3F, G). NFT-bearing cells were frontal pyramidal and parahippocampal neurons. In 2 additional dogs of age 4, tau-positive neurons were seen in the frontal cortex (Figure 3H). In these 2 dogs, weak tau hippocampal neuronal cytoplasmic staining was seen, although the modified Bielschowsky silver stain was negative. Nuclear immunoreactivity to the p65 subunit of NF-κB was present in olfactory bulb neurons at age 2 wk and abundant in cortical neurons and Purkinje, cerebellar granular, and perivascular cortical cells by age 8 months (Figure 4A–C).

The NF-κB protein complex seemed localized in the cytosol of reactive astrocytes in dogs $\geq$1 year, as indicated by the morphological similarity of NF-κB-positive cells and reactive GFAP-positive astrocytes (Figure 4C). NF-κB nuclear positivity was not seen in control dogs. iNOS-positive endothelial cells were first seen at age 4 weeks in SWMMC dogs. Older dogs showed strong positivity in endothelial, glial, and subpial astrocytes, cortical neurons in layers III–V, and the choroid plexus epithelium (Figure 4D, E, G). Strong staining was also observed in hypothalamic, thalamic, and midbrain (substancia nigra) regions, and in pons neurons and blood vessels. In dogs older than 5 years, substancia nigra neurons showed variable degranulation and strong cytoplasmic iNOS staining (Figure 4H). Control dogs older than 6 years showed weak iNOS positivity in endothelial and white matter glial cells.

Electron Microscopy: Frontal sections from control and exposed animals matched by age and gender were examined by transmission electron microscopy. Three early vascular alterations seen clearly in the 1-um, toluidine blue sections in dogs ages 8 months to 3 years included capillary endothelial cells with short anemonae-like processes extending into the lumen of the vessels, focal absence of astrocytic foot processes around small capillaries and arterioles, and intracytoplasmic accumulation of electron-lucent and medium-density lipid droplets in smooth muscle and pericyte cells (Figures 5A–D, 6A–C). Lipid accumulation in the smooth muscle cells of the cortical small arterioles started as small, discrete globules, which fused and became more prominent with the age of the animal (Figure 6D, E). Only scattered cortical arterioles and capillaries could be seen with these lipid structures starting with the 8-month-old SWMMC dog; the oldest 12-year-old dog showed extensive vascular changes with the majority of cortical vessels involved. Similar, more discrete vascular findings were seen in the thalamus, hypothalamus, basal ganglia, midbrain, and cerebellum.

Ultrastructural changes in capillaries showed endothelial cells with increased luminal and abluminal pinocytic vesicles, scanty mitochondria, rough endoplasmic reticulum (RER), and glycogen. Vessels displayed irregular luminal surfaces (Figure 6A). Starting at age 1, astrocytic foot processes were focally absent around the basement membrane (BM) of capillaries and in some areas retracted, leaving a greatly distended perivascular space (Figure 5A, 6A). The absence of focal astrocytic foot processes was common in dogs older than 3 years. Two dogs ages 7 and 12 years displayed partially degranulated intraluminal PMN leucocytes in white matter blood vessels (Figure 6B). Young dogs showed reduplication of the BMs in cortical capillaries, with focal thickening. This change was usually associated with absent, retracted, or disintegrating foot astrocytes. Older dogs (>5 years) displayed isolated red blood cells (RBC) lying in the neuropil around abnormal capillaries (Figure 6C) and increased amounts of lipofuscin in glial cytoplasm (Figure 6F).

Discussion

Healthy canines in Mexico City exhibited early activation of the NF-κB transcription factor and iNOS expression. Canines ages $\leq$1 year showed signs in the olfactory bulbs and frontal capillaries of BBB dysfunction and neuronal chromatolysis and satellitosis in layers III to VI. Reactive astrocytosis, white matter glial cell apoptosis, and strong apoE vascular immunoreactivity were seen in animals older than 1 year. Deposition of lipid droplets in smooth muscle cells and pericytes was observed in dogs $\geq$3 years, and nonneuritic plaques and NFTs were apparent in 4- to 12-year-olds. These dogs also exhibited nasal respiratory and olfactory pathology with a histopathological picture that has been described in experimental animals and humans upon exposure to air pollutants and inhaled toxic substances (20, 54, 85). The breakdown of both the nasal respiratory and the nose-brain olfactory barriers increases the likelihood of diminishing their protective functions and enabling the delivery of potentially toxic inhaled substances (39, 88). The olfactory bulb, a limbic paleocortex that receives monosynaptic sensory efferents from the olfactory mucosa, was involved early in all SWMMC dogs. Capillary pathology was a major finding in the olfactory bulb and frontal cortex. Strong expression of iNOS in endothelial cells and astrocytes, 2 major components of the defensive BBB, was a crucial finding in these dogs. iNOS is transcriptionally regulated by cytokines and redox-sensitive transcriptional factors (94, 104). Nitric oxide can lead to an opening in the BBB (104); in the acute phase of experimental bacterial meningitis, iNOS-derived NO contributes to peroxynitrate formation and BBB breakdown (113). The BBB breaching in these animals was illustrated by the extravasated RBC. Grammas (53) has shown that brain microvessels in AD produce high, potentially toxic levels of nitric oxide that in turn kills neurons.

Brain endothelial cells are important regulators of CNS homeostasis, and EM studies of the BBB in AD patients have demonstrated decreased mitochondrial content, increased pinocytosis, accumulation of collagen, and focal necrotic changes (32). Endothelial cells participate in inflammatory responses and are powerful producers of soluble inflammatory mediators (12, 68, 78). Elevated pinocytosis may increase transcytotic activity of the endothelium, which in turn translates into an increased influx of plasma components, such as low density lipoprotein (LDL), into the subendothelial space (30). Interestingly, nitric oxide (NO) concentrates in lipophilic cell compartments and regulates oxidant-induced lipid oxidation. ApoE plays a central role in the brain response to injury and neurodegeneration (93), and the progressive deposition in smooth muscle cells and pericytes of

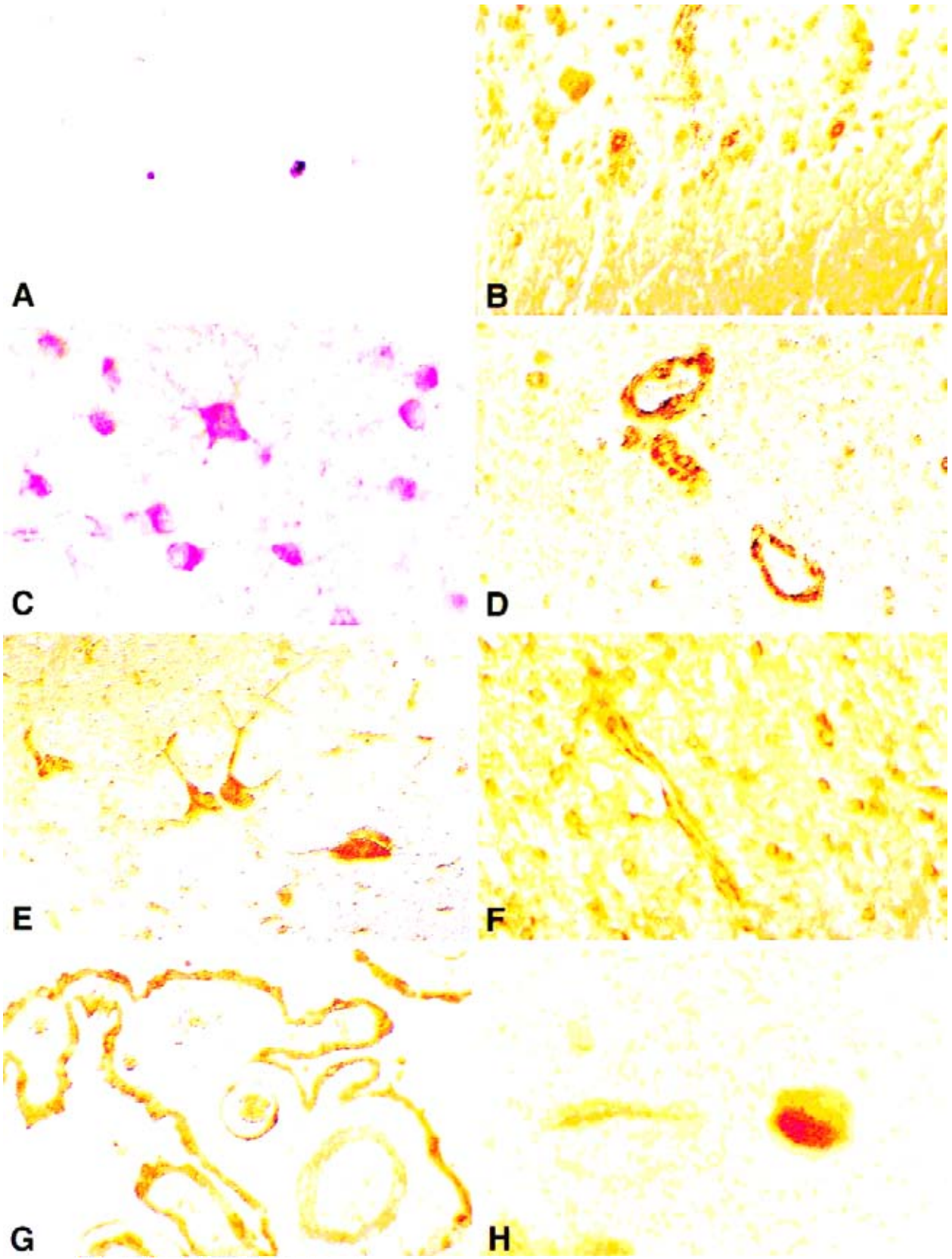

FIGURE 4.—SWMMC dogs. 4A) Frontal cortex, 8-month-old. Nuclear immunoreactivity to the p65 subunit of NF-κB is seen in a neuron and a glial cell. NF-κB with a red substrate. ×214. 4B) Cerebellum, 4-year-old. Nuclear immunoreactivity to the p65 subunit of NF-κB is present in Purkinje cells; nucleoli are negative. Nomarski optics. NF-κB with a brown substrate. ×214. 4C) Frontal white matter, 7-year-old. Cytoplasmic immunoreactivity to the p65 subunit of NF-κB is seen in glial cells, both astrocytes and oligodendrocytes. NF-κB with a red substrate. ×420. 4D) Frontal white matter, 3-month-old. iNOS-positive endothelial cells are seen; note the negativity of the nucleus. Nomarski optics. No counterstain. ×214. 4E) Hypothalamic neurons, 8-month-old. Strong iNOS staining in the cytoplasm. Nomarski optics. No counterstain. ×420. 4F) Frontal white matter, 6-year-old. Immunoreactivity for iNOS is present in the cytoplasm of glial and endothelial cells. No counterstain. ×214. 4G) Choroid plexus, 8-year-old. Strong iNOS immunoreactivity is present in the cytoplasm of the epithelial and endothelial cells. No counterstain, ×107. 4H) Pigmented substantia nigra cell, 6-year-old. A well-granulated cell shows moderate iNOS staining. No counterstain. ×1072.

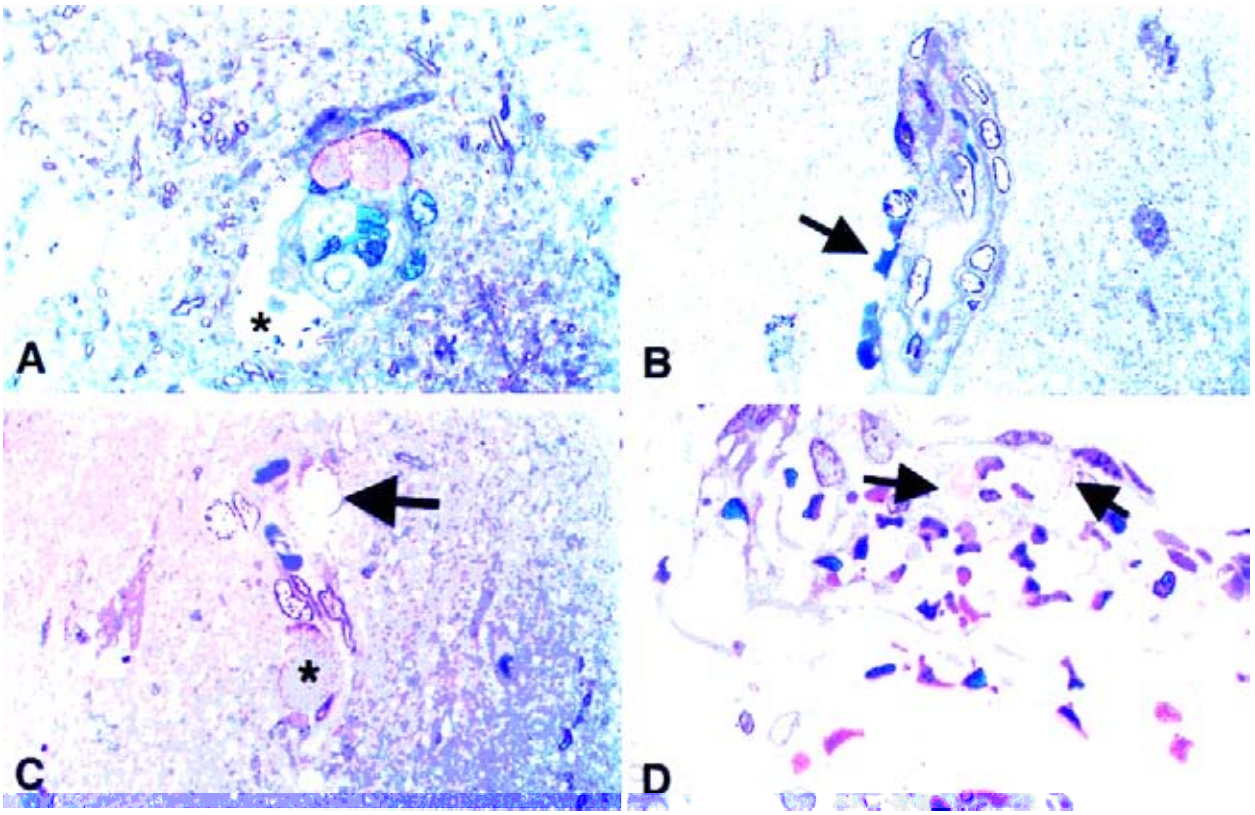

FIGURE 5.—SWMMC dogs. Frontal cortex,1-μm-thick epoxy resin-embedded, toluidine blue-stained sections. 5A) 2-year-old. Small cortical blood vessel shows 2 lipid deposits (white*) in the blood vessel wall. Red blood cells are present in the lumen. Focal absence of astrocytic foot processes and unidentified debri are present around the vessel (black*). ×420. 5B) 6-year-old. Several red blood cells are seen outside the vessel wall (arrow). The nucleus above the arrow shows clumping of the chromatin. Neurons contain lipofuscin pigment. ×420. 5C) 12-year-old. Blood vessel is compressed by large lipid deposit (*). In focal areas the lipid has been partially removed (arrow). An adjacent neuron is shrunken. ×420. 5D) 3-years-old. Frontal leptomeninges. Lipid deposits are present in leptomeningeal blood vessels (arrows) ×420.

immunoreactive apoE in these dogs could be indicative of a dysfunction in lipid transport as seen in AD (93).

Rhodin's inflammatory animal model of vascular inflammation (95) illustrates the effects of a single injection of TNF α, and IL-1β upon the endothelium. IL-1 β-induced damage includes vesiculation of the endothelial cytoplasm, accumulation of plasma lifting smooth muscle cells away from the endothelium, and their association with gaps and discontinuities of the endothelial lining. Rhodin suggested that disruption of the BBB by pro-inflammatory cytokines initiates compensatory responses that alter the normal homeostatic properties of the endothelium. Indeed specific combinations of cytokines (IL1 + TNF α/interferon γ) induced a significant neuronal cell injury in mixed neuron/glial cultures (61). Cytokines in the systemic circulation presumably could stimulate hematopoietic bone marrow cells capable of crossing the BBB to undergo differentiation into brain microglia (42). Microglia become activated and secrete a myriad of inflammatory cascade mediators, including nitric oxide, proteases, arachidonic acid derivatives, reactive oxygen species, and cytokines (4, 8, 14, 29, 49, 80, 103). Moreover, amyloid precursor protein (APP) is a microglial acute phase protein (8, 9). Microglia are present in significant numbers in normal brains, but their distribution is not uniform (70, 89). More microglia are found in the cortex than in the white matter, and densely populated areas include the olfactory telencephalon, hippocampus, basal ganglia, and substancia nigra (70); such distribution may explain the "vulnerability" of these areas (76). Thus, a sustained inflammatory stimulus, such as the one encountered in the lower respiratory tract upon exposure to air pollutants, produces lung endothelial and epithelial injury and cytokine release from both circulating inflammatory and resident lung cells (25). Cytokines present in the systemic circulation have the ability to trigger brain events in cascades leading to different activators of transcription transduction pathways, including kinases/NF-κB in vascular cells of the CNS (97). The brain blood vessels have both constitutive and induced expression of receptors for different proinflammatory ligands (97).

We observed nuclear staining of NF-κB first in olfactory bulb neurons and the frontal cortex, then other cortical regions, Purkinje cells, and perivascular cells. Cytoplasmic staining of cortical and white matter glial cells was also apparent. NF-κB plays a crucial role in regulating cytokine cascades, and functional NF-κB complexes are present in neurons, astrocytes, oligodendroglia, and microglia; NF-κB may be involved in iNOS induction stimulated by cytokines and/or lipopolysaccharide (LPS) in various cell types and tissues (79). Genes encoding injury-responsive cytokines are induced by NF-κB in neurons and glial cells; these include

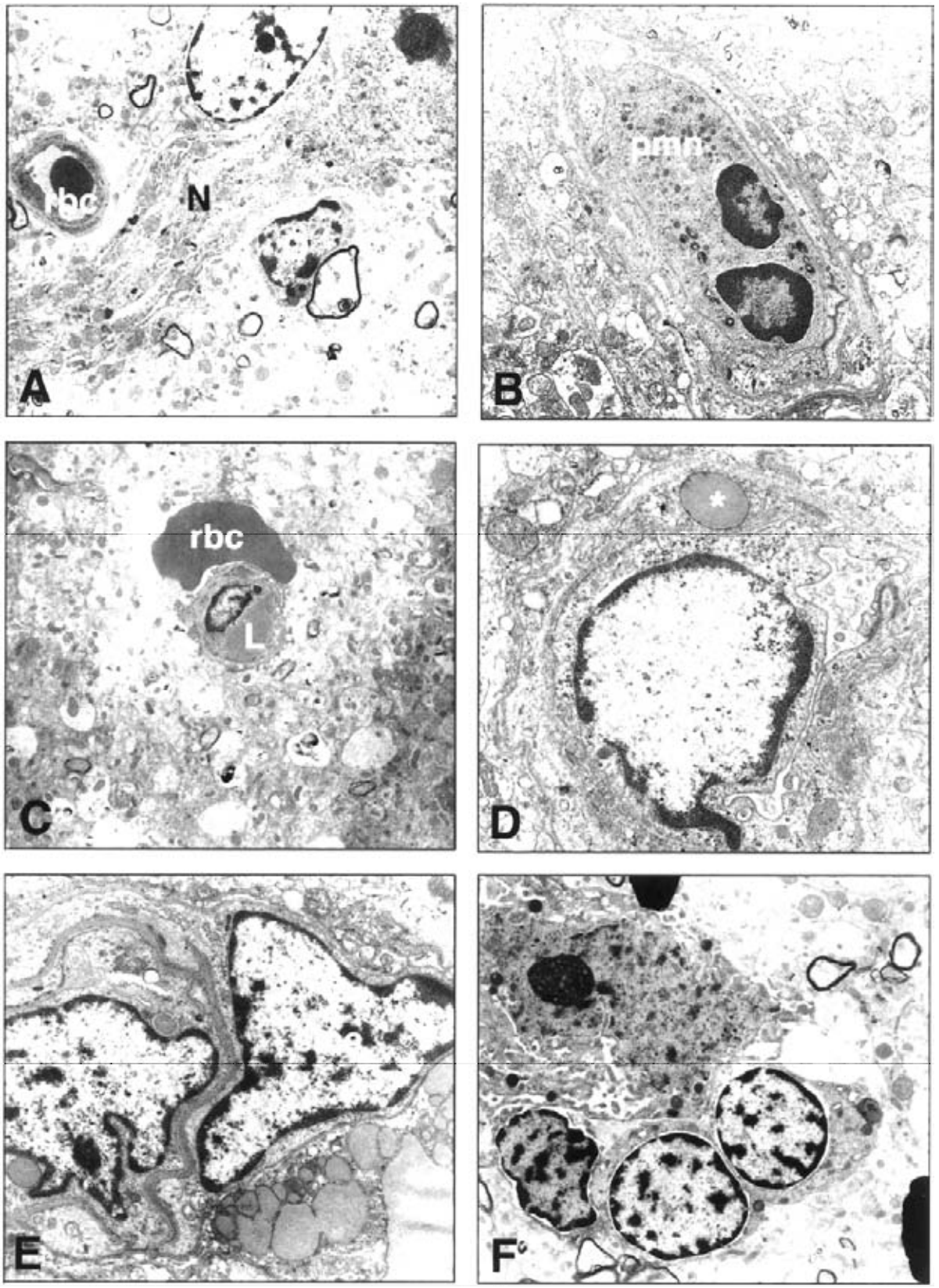

FIGURE 6.—Electron microscopy of frontal sections; SWMMC dogs. 6A) 1-year-old. A large pyramidal neuron (N) is adjacent an oligodendrocyte (O) and an astrocyte (top of picture). Capillary shows luminal RBC and endothelial cell's processes projecting into the lumen. There is focal absence of astrocytic foot processes in a segment of the capillary (*). The oligodendrocyte exhibits lipofuscin and a degenerating axon. ×3000. 6B) 12-year-old male. White matter capillary. A partially degranulated polymorphonuclear leucocyte (pmn) is in close contact with the endothelial surface. ×7000. 6C) 8-year-old female. White matter capillary. RBC lies outside a capillary, its lumen marked (L). Notice the disrupted adjacent neuropil. ×3000. 6D) 3-year-old male. White matter capillary. Note presence of lipid deposit in cytoplasm of a pericyte (*). Capillary lumen is marked L. ×12,000. 6E) 12-year-old male (same as 6B). White matter capillary. Abundant deposits of lipid in cytoplasm of smooth muscle cells (smc). ×7000. 6F) 7-year-old male. Cortex. Three glial cells are seen adjacent to a pyramidal neuron. This neuron shows enhanced affinity for toluidine blue in the 1-μm-thick section. Lipofuscin is seen in glial cytoplasm. ×7000.

TNF α, IL6, and APP (79). High-level activation of NF-κB may promote sustained production of neurotoxins; activation of NF-κB in astrocytes results in increased expression of nitric oxide synthase and increased nitric oxide production—an observation clearly demonstrated in these animals. The enzyme nitric oxide synthase 2 (inducible NOS) is strongly present in glial and endothelial cells, microglia, scattered pyramidal neurons, apoptotic bodies in the white matter, and the choroid plexus epithelium. Both NF-κB activation and iNOS expression are concomitant with white matter glial apoptosis and neuronal satellitosis but precede extensive glial reactivity—evidenced by GFAP upregulation. Acarin et al (1) described activation of NF-κB in severely damage immature rat brain affected by neuronal degeneration and BBB disruption; moreover, this activation preceded astrocytic hypertrophy and GFAP upregulation in a sequence similar to ours. Blockage of persistent NF-κB activation with anti-oxidants (34) is an avenue that can be explored in experimental animals exposed in controlled chambers to air pollutants.

Inflammation clearly occurs in the Alzheimer's brain (3), and damage microcirculation is crucial (38, 52, 53). Based on our findings of inflammation and endothelial damage in these highly exposed dogs, we hypothesize that the initial and perpetuating inflammatory source is primarily the respiratory tract. Events occur so that circulating cytokines have the ability to trigger expression of numerous cytokine receptors in the endothelium of cerebral capillaries; endothelial cells are damage; the BBB is broken; microglia are activated; neurons and glial cells are damage; and the brain perpetuates the inflammatory mechanisms. The appearances of nonneuritic plaques and NFTs are late events in these dogs.

Consistent with our findings in this work are medical evaluations of clinically healthy, well-nourished SWMMC children who exhibit nasal mucosal abnormalities, hyperinflation, and interstitial markings by chest X-ray, spirometric abnormalities, and peripheral blood smears suggestive of bone marrow involvement (23). Moreover, SWMMC children show an imbalance of serum cytokines, and significant positive correlations are seen between TNFα and IL8, IL8 and endothelin, and TNFα and endothelin (23). The radiological abnormalities and spirometric changes suggest the development of small airway disease with the accompanying inflammatory picture and bone marrow effect (23). Sherwin has shown centriacinar inflammatory disease in young individuals residing in Los Angeles and demonstrated significant differences in lung inflammation scores between Miami and Los Angeles residents (102). Thus, chronic lung parenchymal inflammation seems widespread in Mexico City and occurs in at least some young urban residents of the United States.

We observed a significant difference in the number of monocytes between MC and Tlaxcala dogs. Canine monocytosis is associated with infections, trauma, hematologic disorders, stress, autoimmunity, or any disease with significant tissue destruction (100). Monocytopoiesis in the model of thermal injury and sepsis in mice results from an imbalance in myelopoiesis driven by the increased expression of macrophage colony-stimulating factor receptor (116); clearly this avenue of research merits exploration in these canines.

Exposure to complex mixtures of pollutants, predominantly PM and ozone, causes structural changes in the canine lung induced by a sustained inflammatory process and resulting in airway and vascular remodeling and altered repair (22). Ultrafine PM is seen in alveolar type I and II cells, endothelial cells, interstitial macrophages, and intravascular macrophage-like cells. In lung histopathology, PM plays a crucial role, because there is a significant transport of ultrafine PM from the epithelium to the interstitium, and to the endothelial and intravascular compartments in these exposed dogs. Ultrafine particles are associated with stronger inflammatory responses, prolonging of their lung retention, induction of procollagen expression, and increases in airway fibrosis (6, 44, 87). Ultrafine particles less than 0.1 um possess unique physicochemical features (64), are produced by the burning of fossil fuels or photochemical reactions, can easily penetrate into deep lung regions, and are deposited in the lung by diffusion; deposition spreads over large areas of the lung. Enhanced proximal airway deposition for women, both for ultrafine and coarse particles, has been attributed to smaller dimensions of the upper airways, which could result in an increase in inertial impaction (64). Kim and Jaques (64) suggested that, because of complex upper airway geometry and enhanced turbulence, the end result could be an increase in diffusive deposition of ultrafine particles in women. Deposition of PM in head regions, although small ($<3\%$), could become significant if both the respiratory and olfactory barriers are impaired. Further, total lung deposition is greater (5–15%) in women than men. Women receive a greater dose of ultrafine particles in the head and tracheobronchial regions (64).

Particulate matter concentrations in Mexico City are above the US current standards for most of the metropolitan area, and a persistent haze blankets the city, especially in the winter. Heavy metals in the atmosphere are present in aerosol form, primarily as metal oxide particulates. A cluster typically identified with fuel oil includes Cr, Ni, V, and S, and high correlations are found between Zn, Cu, and Mn elements associated with industry or traffic (83). The traffic contribution of metals is present only in the fine PM fraction (83). Carbon-containing aerosols account for 20 to 35% of the PM_{10} and 25 to 50% of the $PM_{2.5}$. The additional chemical layering of a carbon core by nitrates, sulfates, and other organic materials and metals such as iron causes greater local oxidative damage than the vaporized state (17). Another aspect of pollution in MC that could be relevant to nasal/brain pathology is the presence of organic dusts, lipopolysaccharides (LPS), and endotoxins in PM_{10} (15); a large contributor is the 500 tons of canine fecal material deposited daily on the streets.

Injection of the bacterial endotoxin LPS into the hippocampus, cortex, or substancia nigra of adult rats produces substancia nigra degeneration (65); in mixed astrocytic and microglial cell-culture systems, the addition of LPS and cytokines causes upregulation of iNOS in microglia cells (94), and LPS increases nuclear translocation of NF-κB in microglia (56). Intraperitoneal injection of LPS in rats induces endothelial and astrocytic iNOS formation (60).

Regulation and assessment of pollution have focused on ambient concentrations; however, indoor pollution is significant and represents an important contribution to overall PM exposure (62, 109, 112). High indoor $PM_{2.5}$ concentrations are related to tobacco exposure, cooking activities, the use

of air fresheners, and contaminated particle board materials (63, 106, 109, 112). A comparison of worldwide epidemiological studies shows that both the incidence and prevalence figures for dementia increase with age and that women have a higher risk for developing AD according to every report available in the literature (7, 46, 74, 101). There are also significant differences in incidence and prevalence around the world (74, 101, 110). The increased risk of AD, as well as PD, with lower literacy (50, 90) could be related to exposure to toxins and PM in the environment, starting in childhood, and occupational history involving exposure to iron, copper, manganese, mercury, zinc, and lead (51). The higher risk for women could be related to the greater dose of ultrafine particles in their heads, total lung deposition, nasal anatomy with anterior distribution in the olfactory epithelium (71), household exposures (cooking habits), and decreased levels of neuroprotective steroidal structures after menopause (10).

Microglial activation is a central element in CNS demyelination (115). The prevalence of multiple sclerosis has doubled in Mexico City in the last 10 years, and 70% of patients are females (35). Data on the incidence and prevalence of AD and PD are not available from reliable sources in Mexico City; however, empirical observations point toward an increase in their incidence in the last decade (personal communication, Patricia Mendoza MD, Mexico City, May, 2001).

Nasal findings in this work emphasize the potential impact of upper respiratory physiology and metabolic xenobiotic detoxification (11, 19, 37, 62, 69) upon inhaled gases and materials in the nose when the barriers are no longer intact. SWMMC children and canines show indirect evidence of attempts to restore and protect the nasal epithelium against the effects of continuous exposure to inhaled pollutants (27). Ultrafine PM deposition in nasal epithelial cells and intercellular spaces, the transudate between epithelial cells in nasal biopsies from healthy children in SWMMC (27), and the significant damage to the respiratory and olfactory epithelia in canines highlight the importance of nasal tissues in the study of neurodegenerative diseases. Elucidating the relationship(s) between nasal and brain pathology remains an important task. The chronic inflammatory process elicited within the respiratory tract upon exposure to outdoor and indoor air pollutants (2, 33, 40, 45, 48, 73) could serve as the trigger for a chain of events involving the brain.

In summary, we have described canines chronically exposed to significant concentrations of ozone, PM, and a myriad of other air pollutants. These animals exhibited early and persistent activation of NF-κB, strong expression of iNOS, and alterations in the BBB in cortical capillaries. Degenerating cortical dark, shrunken neurons exhibited prominent satellitosis and were surrounded by apoptotic glial cells, although no apoptosis was identified in the neurons themselves. The paucity of frontal neurons even in young dogs and the evidence of dysfunctional lipid transport in vascular smooth muscle cells and pericytes were striking. The histopathology we observed in these urban dogs is of sufficient magnitude to warrant concern that similar histopathology may be occurring in humans residing in large polluted metropolitan areas. If so, these alterations could provide insight into the underlying early pathophysiological mechanisms responsible for neurodegenerative diseases such as Alzheimer's and Parkinson's.

ACKNOWLEDGMENTS

We are grateful to Dr. Brooke Mossman, Professor, Pathology Department, University of Vermont, Burlington, for her comments and encouragement. We also express appreciation to Dr. Hillel S. Koren from the National Health and Environmental Effects Research Laboratory, US Environmental Protection Agency, and Dr. Milan J. Hazucha, Dr. William Reed, Dr. Terry van Dyke, Robert Schoonhoven, and Luisa Brighton from the University of North Carolina at Chapel Hill for their support. We thank JoAnne Johnson for her patience and thoroughness in editing the manuscript. This work was supported in part by NIEHS Training Grants T32ESO7126 and the Env Path ESO7017 and P30ES10126.

REFERENCES

1. Acarin L, Gonzalez B, Castellano B (2000). STAT3 and NF κB activation precedes glial reactivity in the excitotoxically injured young cortex but not in the corresponding distal thalamic nuclei. *J Neuropath Exp Neurol* 59: 151–163.
2. Adamson IY, Vincent R, Bjarnason SG (1999). Cell injury and interstitial inflammation in rat lung after inhalation of ozone and urban particles. *Am J Respir Cell Mol Biol* 20: 1067–1072.
3. Akiyama H, Barger S, Barnum S, Bradt B, Bauer J, Cole GM, Cooper NR, Eikelenboom P, Emmerling M, Fiebich BL, Finch CE, Frautschy S, Griffin WS, Hampel H, Hull M, Landreth G, Lue L, Mrak R, Mackenzie IR, McGeer PL, O'Banion MK, Pachter J, Pasinetti G, Plata-Salaman C, Rogers J, Rydel R, Shen Y, Streit W, Stromeyer R, Tooyoma I, Van Muiswonkel FL, Veerhuis R, Walker D, Webster S, Wegrzyniak B, Wenk G, Wyss-Coray T (2000). Inflammation and Alzheimer's disease. *Neurobiol Aging* 21: 383–421.
4. Aloisi F (1999).The role of microglia and astrocytes in CNS immune surveillance and immunopathology. *Adv Exp Med Biol* 468: 123–133.
5. Baez AP, Belmont R, Padilla H (1995). Measurements of formaldehyde and acetaldehyde in the atmosphere of Mexico City. *Environ Pollut* 89: 163–167.
6. Baeza-Squiban A, Bonvallot V, Boland S, Marano F (1999). Airborne particles evoke an inflammatory response in human airway epithelium. Activation of transcription factors. *Cell Biol Toxicol* 15: 375–380.
7. Bachman DL, Wolf PA, Linn RT, Knoefel JE, Cobb JL, Belanger AJ, White LR, D'Agostino RB (1993). Incidence of dementia and probable Alzheimer's disease in a general population: The Framingham study. *Neurology* 43: 515–519.
8. Banati RB, Gehrmann J, Czech C, Monning U, Jones LL, Konig G, Beyreuther K, Kreutzberg GW (1993). Early and rapid de novo synthesis of Alzheimer beta A4-amyloid precursor protein (APP) in activated microglia. *Glia* 9: 199–210.
9. Banati RB, Gehrmann J, Monning U, Czech C, Beyreuther K, Kreutzberg GW (1994). Amyloid precursor protein (APP) as a microglial acute phase protein. *Neuropath Appl Neurobiol* 20: 194–195.
10. Behl C, Moosmann B, Manthey D, Heck S (2000). The female sex hormone oestrogen as neuroprotectant: Activities at various levels. *Novartis Found Symp* 230: 221–234.
11. Bennett WD, Zeman KL, Kang CW, Schechter MS (1997). Extrathoracic deposition of inhaled, coarse particles (4.5 um) in children vs adults. *Ann Occup Hyg* 41: 497–502.
12. Bevilacqua MP, Gimbrone MA (1987). Inducible endothelial functions in inflammation and coagulation. *Semin Thromb Hemost* 13: 425–433.
13. Blake DR, Rowland FS (1995). Urban leakage of liquefied petroleum gas and its impact on Mexico City air quality. *Science* 269: 953–956.
14. Boje KM, Arora PK (1992). Microglial-produced nitric oxide and reactive oxides mediate neuronal cell death. *Brain Res* 587: 250–256.
15. Bonner JC, Rice AB, Lindroos PM, O'Brien PO, Dreher KL, Rosas I, Alfaro-Moreno E, Osornio-Vargas AR (1998). Induction of the lung myofibroblast PDGF receptor system by urban ambient particles from Mexico City. *Am J Respir Cell Mol Biol* 19: 672–680.

16. Borras D, Ferrer I, Pumarola M (1999). Age-related changes in the brain of the dog. *Vet Pathol* 36: 202–211.
17. Brandli O (1996). Are inhaled dust particles harmful for our lungs? *Schweiz Med Wochenschr* 126: 2165–2174.
18. Bravo H, Camacho R, Roy-Ocotla G, Sosa R, Torres R (1991). Analysis of the change in atmospheric urban formaldehyde and photochemistry activity as a result of using methyl-*t*-butyl ether (MTBE) as an additive in gasolines in the metropolitan area of Mexico City. *Atmos Environ* 25: 285–288.
19. Bukowski JA, Wartenberg D, Goldschmidt M (1998). Environmental causes for sinonasal cancers in pet dogs, and their usefulness as sentinels of indoor cancer risk. *J Toxicol Environ Health* 54: 579–591.
20. Calderón-Garcidueñas L, Gambling TM, Acuña H, Garcia R, Osnaya N, Monroy S, Villarreal-Calderón A, Carson J, Koren HS, Devlin RB (2001c). Canines as sentinel species for assessing chronic exposures to air pollutants: Part 2. Cardiac pathology. *Toxicol Sci* 61: 356–367.
21. Calderón-Garcidueñas L, Mora-Tiscareño A, Chung CJ, Valencia G, Fordham LA, Garcia R, Osnaya N, Romero L, Acuña H, Villarreal-Calderón A, Devlin RB, Koren HS (2000). Exposure to air pollution is associated with lung hyperinflation in healthy children and adolescents in Southwest Mexico City. A Pilot Study. *Inhalation Toxicol* 12: 537–556.
22. Calderón-Garcidueñas L, Mora-Tiscareño A, Fordham LA, Chung CJ, Garcia R, Osnaya N, Hernandez J, Acuña H, Gambling TM, Villarreal-Calderón A, Carson J, Koren HS, Devlin RB (2001b). Canines as sentinel species for assessing chronic exposures to air pollutants: Part 1. Respiratory pathology. *Toxicol Sci* 61: 342–355.
23. Calderón-Garcidueñas L, Mora A, Fordham LA, Valencia G, Chung CJ, Villarreal-Calderón A, Koren HS, Devlin RB, Hazucha MJ (2001d). Lung damage and cytokine profile in children chronically exposed to air pollutants. *Am J Respir Crit Care Med* 163: A884.
24. Calderón-Garcidueñas L, Osorno-Velazquez A, Bravo-Alvarez H, Delgado-Chavez R, Barrios-Marquez R (1992). Histopathological changes of the nasal mucosa in Southwest Metropolitan Mexico City. *Am J Pathol* 140: 225–232.
25. Calderón-Garcidueñas L, Osnaya N, Rodríguez-Alcaraz A,Villarreal-Calderón A (1997). DNA damage in nasal respiratory epithelium from children exposed to urban pollution. *Environ Mol Mut* 30: 11–20.
26. Calderón-Garcidueñas L, Rodríguez-Alcaraz A, Villarreal-Calderón A, Lyght O, Janszen D, Morgan KT (1998). Nasal epithelium as a sentinel for airborne environmental pollution. *Toxicol Sci* 46: 352–364.
27. Calderón-Garcidueñas L,Valencia-Salazar G, Rodríguez-Alcaraz A, Gambling TM, García R, Osnaya N, Villarreal-Calderón A, Devlin RB, Carson JL (2001a). Ultrastructural nasal pathology in children chronically and sequentially exposed to air pollutants. *Am J Respir Cell Mol Biol* 24: 132–138.
28. Cano D (2001). Heces caninas grave problema de salud. El Universal, Mexico City, May 17: 4.
29. Chao CC, Hu S, Moliter TW, Shaskan EG, Peterson PK (1992). Activated microglia mediate cell injury via a nitric oxide mechanism. *J Immunol* 149: 2736–2741.
30. Chao SE, Lee RS, Shih SH, Chen JK (1998). Oxidized LDL promotes vascular endothelial cell pinocytosis via a prooxidation mechanism. *Faseb J* 12: 823–830.
31. Cicero-Fernández P, Thistlewaite WA, Falcon YI, Guzman IM (1993). TSP, PM_{10} and PM_{10}/TSP ratios in the Mexico City Metropolitan Area: A temporal and spatial approach. *J Exp Anal Environ Epidemiol* 3: 1–14.
32. Claudio L (1996). Ultrastructural features of the blood–brain barrier in biopsy tissue from Alzheimer's disease patients. *Acta Neuropath* 91: 6–14.
33. Clarke RW, Coull B, Reinisch U, Catalano P, Killingsworth CR, Koutrakis P, Kavouras I, Godleski JJ (2000). Inhaled concentrated ambient particles are associated with hematologic and bronchioalveolar changes in canines. *Environ Health Perspect* 108: 1179–1187.
34. Clemens JA (2000). Cerebral ischemia: Gene activation, neuronal injury, and the protective role of antioxidants. *Free Radic Biol Med* 28: 1526–1531.
35. Corona T, Rodrígues JL, Otero E, Stopp L (1996). Multiple sclerosis in Mexico: Hospital cases at the National Institute of Neurology and Neurosurgery, Mexico City. *Neurología* 11: 170–173.
36. Cummings BJ, Head E, Ruehl W, Milgram NW, Cotman CW (1996). Canine as an animal model of human aging and dementia. *Neurobiol Aging* 17: 259–268.
37. Dahl AR, Lewis JL (1993). Respiratory tract uptake of inhalants and metabolism of xenobiotics. *Annu Rev Pharmacol Toxicol* 33: 383–407.
38. de la Torre J (2000). Cerebral hypoperfusion, capillary degeneration, and development of Alzheimer disease. *Alzheimer Dis Assoc* 14: 572–581.
39. Divine KK, Lewis JL, Grant PG, Bench G (1999). Quantitative particle-induced X ray emission imaging of rat olfactory epithelium applied to the permeability of rat epithelium to inhaled aluminum. *Chem Res Toxicol* 12: 575–581.
40. Driscoll KE, Carter JM, Hassenbein DG, Howard B (1997). Cytokines and particle-induced inflammatory cell recruitment. *Environ Health Perspect* 105: 1159–1164.
41. Edgerton SA, Bian X, Doran JC, Fast JD, Hubbe JM, Malone EL, Shaw WJ, Whiteman CD, Zhong S, Arriaga JL, Ortiz E, Ruiz M, Sosa G, Vega E, Limon T, Guzman F (1999). Particulate air pollution in Mexico City: A collaborative research project. *Air Waste Manag Assoc* 49: 1221–1229.
42. Eglitis MA, Mezey E (1997). Hematopoietic cells differentiate into both microglia and macroglia in the brains of adult mice. *Proc Nat Acad Sci USA* 94: 4080–4085.
43. Fast DJ, Zhong S (1998). Metereological factors associated with inhomogeneous ozone concentrations with the Mexico Basin. *J Geophysical Res* 103(D15): 18927–18946.
44. Ferin J, Oberdörster G, Penney DP (1992). Pulmonary retention of ultrafine and fine particles in rats. *Am Respir Cell Mol Biol* 6: 535–542.
45. Finkelstein JN, Johnston C, Barrett T, Oberdörster G (1997). Particulate-cell interactions and pulmonary cytokine expression. *Environ Health Perspect* 105S: 1179–1182.
46. Fratiglioni L, De Ronchi D, Aguero-Torres H (1999). Worldwide prevalence and incidence of dementia. *Drugs Aging* 15: 365–375.
47. García-Gutierrez A, Herrera-Hernandez M, Bravo-Alvarez H (1991). Campus ozone concentrations related to new blends in gasoline sold in Mexico City. A statistical analysis. *Air Waste Management Assoc* A115-4.
48. Ghio AJ, Kim C, Devlin RB (2000). Concentrated ambient air particles induce mild pulmonary inflammation in healthy human volunteers. *Am J Respir Crit Care Med* 162: 981–988.
49. Giulian D (1999). Microglia and the immune pathology of Alzheimer disease. *Am J Hum Genet* 65: 13–18.
50. Glatt SL, Hubble JP, Lyons K, Paolo A, Toster AI, Hassanein RE, Koller WC (1996). Risk factors for dementia in Parkinson's disease: Effect of education. *Neuroepidemiology* 15: 20–25.
51. Gorell JM, Johnson CC, Rybicki BA, Peterson EL, Kortsha GX, Brown GG, Richardson RJ (1997). Occupational exposure to metals as risk factors for Parkinson's disease. *Neurology* 48: 650–658.
52. Grammas P (2000). A damaged microcirculation contributes to neuronal cell death in Alzheimer's disease. *Neurobiol Aging* 21: 199–205.
53. Grammas P, Botchlet TR, Moore P, Weigel PH (1997). Production of neurotoxic factors by brain endothelium in Alzheimer's disease. *Ann NY Acad Sci* 826: 47–55.
54. Hardisty JF, Garman RH, Harkema JR, Lomax LG, Morgan KT (1999). Histopathology of nasal olfactory mucosa from selected inhalation toxicity studies conducted with volatile chemicals. *Toxicol Path* 27: 618–627.
55. Henriksson J, Tjälve H (2000). Manganese taken up into the CNS via the olfactory pathway in rats affects astrocytes. *Toxicol Sci* 55: 392–398.
56. Heyen JR, Ye S, Finck BN, Johnson RW(2000). Interleukin (IL)-10 inhibits IL-6 production in microglia by preventing activation of NF-κB. *Brain Res Mol Brain Res* 77: 138–147.
57. Hirai T, Kojima S, Shimada A, Umemura T, Sakai M, Itakura C (1996). Age-related changes in the olfactory system of dogs. *Neuropath Appl Neurobiol* 22: 531–539.
58. Hock C, Golombowski S, Muller-Spahn F, Peschel O, Riederer A, Probst A, Mandelkow E, Unger J (1998). Histological markers in nasal mucosa of patients with Alzheimer's disease. *Eur Neurol* 40: 31–36.

59. Hoffman HJ, Ishii EK, MacTurk RH (1998). Age-related changes in the prevalence of smell/taste problems among the United States adult population. Results of the 1994 disability supplement to the National Health Interview Survey (NHIS). *Ann NY Acad Sci* 855: 716–722.
60. Iwase K, Miyanaka K, Shimizu A, Nagasaki A, Gotoh T, Mori M, Takiguchi M (2000). Induction of endothelial nitric-oxide synthase in rat brain astrocytes by systemic lipopolysaccharide treatment. *J Biol Chem* 275: 11929–11933.
61. Jeohn GH, Kong LY, Wilson B, Hudson P, Hong JS (1998). Synergistic neurotoxic effects of combined treatments with cytokines in murine primary mixed neuron/glia cultures. *J Neuroimmunol* 85: 1–10.
62. Johnson EW (2000). Immunocytochemical characteristics of cells and fibers in the nasal mucosa of young and adult macaques. *Anat Rec* 259: 215–228.
63. Johnson T, Long T, Ollison W (2000). Prediction of hourly microenvironmental concentrations of fine particles based on measurements obtained from the Baltimore scripted activity study. *J Expo Anal Environ Epidemiol* 10: 403–411.
64. Kim CS, Jaques PA (2000). Respiratory dose of inhaled ultrafine particles in healthy adults. *Phil Trans R Soc Lond* 358: 2693–2705.
65. Kim WG, Mohney RP, Wilson B, Jeohn GH, Hong JS (2000). Regional difference in susceptibility to lipopolysaccharide-induce d neurotoxicity in the rat brain: Role of microglia. *J Neurosci* 20: 6309–6316.
66. Kovacs T, Cairns NJ, Lantos PL (1999). Beta-amyloid deposition and neurofibrillary tangle formation in the olfactory bulb in ageing and Alzheimer's disease. *Neuropath Appl Neurobiol* 25: 481–491.
67. Kovacs T, Cairns NJ, Lantos PL (2001). Olfactory centres in Alzheimer's disease: Olfactory bulb is involved in early Braak's stages. *Neuroreport* 12: 285–288.
68. Krishnaswamy G, Kelley J, Yerra L, Smith JK, Chi DS (1999). Human endothelium as a source of multifunctional cytokines: Molecular regulation and possible role in human disease. *J Interferon Cytokine Res* 19: 91–104.
69. Larsson P, Tjälve H (2000). Intranasal instillation of aflatoxin B_1 in rats: Bioactivation in the nasal mucosa and neuronal transport to the olfactory bulb. *Toxicol Sci* 55: 383–391.
70. Lawson LJ, Perry VH, Dri P, Gordon S (1990). Heterogeneity in the distribution and morphology of microglia in the normal adult mouse brain. *Neuroscience* 39: 151–170.
71. Leopold DA, Hummel T, Schwob JE, Hong SC, Knecht M, Kobal G (2000). Anterior distribution of human olfactory epithelium. *Laryngoscope* 110: 417–421.
72. Levin S, Bucci TJ, Cohen SM, Fix AS, Hardisty JF, LeGrand EK, Maronpot RR, Trump BF (1999). The nomenclature of cell death: Recommendations of an ad hoc Committee of the Society of Toxicologic Pathologists. *Toxicol Pathol* 27: 484–490.
73. Li XY, Gilmour PS, Donaldson K, MacNee W (1996). Free radical activity and proinflammatory effects of particulate air pollution (PM_{10}) in vivo and in vitro. *Thorax* 51: 1216–1222.
74. Llibre JJ, Guerra MA, Perez-Cruz H, Bayarré H, Fernández-Ramírez S, Gonzalez-Rodríguez M, Samper JA (1999). Dementia syndrome and risk factors in adults older than 60 years old residing in Habana. *Rev Neurol* 29: 908–911.
75. Lin DM, Ngai J (1999). Development of the vertebrate main olfactory system. *Curr Opin Neurobiol* 9: 74–78.
76. Liu B, Wang K, Gao HM, Mandavilli B, Wang JY, Hong JS (2001). Molecular consequences of activated microglia in the brain: Overactivation produces apoptosis. *J Neurochem* 77: 182–189.
77. Los Alamos National Laboratory, US Department of Energy (2001). library@lanl.gov. Mexico City Air Quality Research Initiative Vol II, LA-12699 UC-902 June 1994 pl-S9.
78. Luscher TF, Barton M (1997). Biology of the endothelium. *Clin Cardiol* 20: II-3–II-10.
79. Mattson MP, Camandola S (2001). NF-κB in neuronal plasticity and neurodegenerative disorders. *J Clin Inves* 107: 247–254.
80. McGeer PL, Itagaki S, Boyes BE, McGeer EG (1988). Reactive microglia are positive for HLA-DR in the substancia nigra of Parkinson's and Alzheimer's disease brains. *Neurology* 38: 1285–1291.
81. Meneses F, Romieu I, Ramirez M, Colome S, Fung K, Ashley D, Hernandez-Avila MA (1999). Survey of personal exposures to benzene in Mexico City. *Arch Environmental Health* 54: 359–363.
82. Meyer H (1964). The brain. In: *Anatomy of the Dog*, Miller ME (ed). WB Saunders Company, Philadelphia, PA, pp 480–532.
83. Miranda J, Andrade E, Lopez-Suarez A, Ledesma R, Cahill TA, Wakabayashi PH (1996). A receptor model for atmospheric aerosols from a southwestern site in Mexico City. *Atmospheric Environ* 30: 3471–3479.
84. Morgan KT (1991). Nasal dosimetry, lesion distribution and the toxicologic pathologist: A brief review. *Toxicol Pathol* 19: 337–351.
85. Morgan KT, Monticello TM (1990). Airflow, gas deposition, and lesion distribution in the nasal passages. *Environ Health Perspect* 85: 209–218.
86. Nakashima T, Tanaka M, Inamitsu M, Uemura T (1991). Immunohistopathology of variations of human olfactory mucosa. *Eur Arch Otorhinolaryngol* 248: 370–375.
87. Nemmar A, Delaunois A, Nemery B, Dessy-Doize C, Beckers JF, Sulon J, Gustin P (1999). Inflammatory effects of intratracheal instillation of ultrafine particles in the rabbit: Role of C-fiber and mast cells. *Toxicol Appl Pharmacol* 160: 250–261.
88. Okuyama S (1997). The first attempt at radioisotopic evaluation of the integrity of the nose-brain barrier. *Life Sci* 60: 1881–1884.
89. Ong WY, Leong SK, Garey LJ, an KK, Zhang HF (1995). A light and electron microscopic study of HLA-DR positive cells in the human cerebral cortex and subcortical white matter. *J Hirnforch* 36: 553–563.
90. Ott A, Breteler MM, van Harskamp F, Clauss JJ, van der Cammen TJ, Grobbee DE, Hofman A (1995). Prevalence of Alzheimer's disease and vascular dementia: Association with education. The Rotterdam study. *BMJ* 310: 970–973.
91. Paik SI, Lehman MN, Seiden AM, Duncan HJ, Smith DV (1992). Human olfactory mucosa. The influence of age and receptor distribution. *Arch Otolaryngol Head Neck Surg* 118: 731–738.
92. Panel on Euthanasia (1993). *J Am Vet Med Assoc* 202: 229–249.
93. Poirier J (2000). Apolipoprotein E and Alzheimer's disease. A role in amyloid catabolism. *Ann NY Acad Sci* 924: 81–90.
94. Possel H, Noack H, Putzke J, Wolf G, Sies H (2000). Selective upregulation of inducible nitric oxide synthase (iNOS) by lipopolysaccharide (LPS) and cytokines in microglia: In vitro and in vivo studies. *Glia* 32: 51–59.
95. Rhodin J, Thomas T, Bryant M, Clark L, Sutton ET (1999). Animal model of vascular inflammation. *J Submicros Cytol Pathol* 31: 305–311.
96. Riveros-Rosas H, Pfeifer GD, Lynam DR, Pedroza JL, Julian-Sanchez A, Canales O, Garfias J (1997). Personal exposure to elements in Mexico City Air. *Sci Total Environ* 198: 79–96.
97. Rivest S, Lacroix S, Vallieres L, Nadeau S, Zhang J, Laflamme N (2000). How the blood talks to the brain parenchyma and the paraventricular nucleus of the hypothalamus during systemic inflammatory and infectious stimuli. *Proc Soc Exp Biol Med* 223: 22–38.
98. Ruehl WW, Bruyette DS, DePaoli A, Cotman CW, Milgram NW, Cummings BJ (1995). Canine cognitive dysfunction as a model for human age-related cognitive decline, dementia and Alzheimer's disease: Clinical presentation, cognitive testing, pathology and response to 1-deprenyl theraphy. *Prog Brain Res* 106: 217–225.
99. Russell MJ, Bobik M, White RG, Hou Y, Benjamin SA, Geddes JW (1996). Age-specific onset of beta-amyloid in beagle brains. *Neurobiol Aging* 17: 269–273.
100. Santangelo S, Gamelli RL, Shankar R (2001). Myeloid commitment shift toward monocytopoiesis after thermal injury and sepsis. *Ann Surg* 233: 97–106.
101. Satou T, Cummings BJ, Head E, Nielson KA, Khan FF, Milgram NW, Velazquez P, Cribbs DH, Tenner AJ, Cotman CW (1997). The progression of beta-amyloid deposition in the frontal cortex of the ages canine. *Brain Res* 774: 35–43.
102. Sherwin R, Richters V, Kraft P, Richters A (2000). Centriacinar region inflammatory disease in young individuals: A comparative study of Miami and Los Angeles residents. *Virchows Arch* 437: 422–428.

103. Streit WJ (2000). Microglial response to brain injury: A brief synopsis. *Toxicol Pathol* 28: 28–30.
104. Thiel VE, Audus KL (2001). Nitric oxide and blood–brain barrier integrity. *Antioxid Redox Signal* 3: 273–278.
105. Uchino T, Kida M, Baba A, Ishii K, Okawa N, Hayashi Y, Shu-miya S (1995). Senile dementia in aged dogs and the diagnostic standards. *Biomed Gerontol* 19: 24–31.
106. van Winkle MR, Scheff PA (2001). Volatile organic compounds, polycyclic aromatic hydrocarbons and elements in the air of ten urban homes. *Indoor Air* 11: 49–64.
107. Villaclara G, Cantoral T (1986). Avances en la investigación de liquenes epifitos como indicadores de contaminación atmosférica en el Valle de México. Memorias del Curso IV Simposio Internacional sobre Biología de la Contaminación, México DF, pp 30–31.
108. Villalobos-Pietrini R, Blanco S, Gomez-Arroyo S (1995). Mutagenicity assessment of airborne particles in Mexico City. *Atmospheric Environ* 89: 163–167.
109. Wainman T, Zhang J, Weschler CJ, Lioy PJ (2000). Ozone and limonene in indoor air: A source of submicron particle exposure. *Environ Health Perspect* 108: 1139–1145.
110. Wang W, Wu S, Cheng X, Dai H, Ross K, Du X, Yin W (2000). Prevalence of Alzheimer's disease and other dementing disorders in an urban community of Beijing, China. *Neuroepidemiology* 19: 194–200.
111. Wegiel J, Wisniewski HM, Dziewiatkowski J, Tarnawski M, Dziewiatkowska A, Morys J, Soltysiak Z, Kim KS (1996). Subpopulation of dogs with severe brain parenchymal beta amyloidosis distinguished with cluster analysis. *Brain Res* 728: 20–26.
112. Williams R, Suggs J, Zweidinger R, Evans G, Creason J, Kwok R, Rodes C, Lawles P, Sheldon L (2000). The 1998 Baltimore particulate matter epidemiology-exposur e study: Part 1. Comparison of ambient, residential outdoor, indoor and apartment particulate matter monitoring. *J Expo Anal Environ Epidemiol* 10: 518–532.
113. Winkler F, Koedel U, Kastenbauer S, Pfister HW (2001). Differential expression of nitric oxide synthases in bacterial meningitis: Role of the inducible isoform for blood-brain barrier breakdown. *J Infect Dis* 183: 1749–1759.
114. Wszolek ZK, Markopoulou K (1998). Olfactory dysfunction in Parkinson's disease. *Clin Neurosci* 5: 94–101.
115. Xiao BG, Link H (1999). Is there a balance between microglia and astrocytes in regulating Th_1/Th_2-cell responses and neuropathologies? *Immunol Today* 29: 477–479.
116. Zinkl JG (1981). The leukocytes. *Vet Clin North Am Small Anim Pract* 11: 237–263.